A morphometric and alignment analysis of volcanic seamounts to determine stress directions, northwestern Ross Sea, Antarctica

Senior Thesis
Submitted in partial fulfillment of the requirements for the
Bachelor of Science Degree
At The Ohio State University

By

Loren Andrew Rosenbeck
The Ohio State University
2013

Approved by

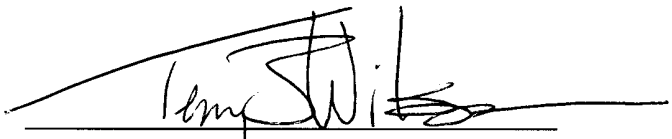

Terry J. Wilson, Advisor
School of Earth Sciences

Table of Contents

- Abstract……....ii
- Introduction……..1
- Geologic Setting……...3
- Methods
    - Determining Stress Directions from Volcanic Cone and Fissure Alignments……8
    - Using Seafloor Multibeam Bathymetry Data to map Volcanic Alignments……...8
        - Bathymetry Data: acquisition and processing
        - Fledermaus and ArcGIS: Image Enhancement and Tools for Mapping
        - Selecting Alignments and testing Alignment Reliability
- Results
    - Improved Mapping with Digital Bathymetry……24
        - Enhanced Image Types
        - Morphologic Provinces of the Adare Bight
        - Seamount Morphology
    - Volcanic Alignment Trends……...27
- Conclusions……....35
- Acknowledgements…….....36
- References……..37

Abstract

Linear arrangements of monogenetic volcanic vents represent important sources for stress and strain data. These volcanic alignments form in platform volcanic fields due to separated eruptions along the trend of fissures fed by subsurface feeder dikes. Subsurface feeder dikes and their surface volcanic vents form alignments parallel to the maximum horizontal stress direction and perpendicular to the minimum horizontal stress in the upper crust, either due to formation of new, magmatically-induced cracks or by the exploitation of suitably oriented preexisting fractures. This research focuses on mapping volcanic vent alignments of a platform volcanic field on the Ross Sea floor in Antarctica. A new method for systematic mapping of vent alignments and elongate vents using multibeam bathymetry is developed. A morphometric analysis of each volcanic vent was completed to provide constraints for mapping the trend of the underlying fissure. Parameters including the measurement of the axial ratio of vent base shape, standard deviation of orthogonal distances from the best fit line connecting vents, standard angular deviation of the vent long axes from the trend of the best fit line, and the average distance between cones were used to test the reliability of each alignment. Mapped alignments have a dominant NE-SW trend, documenting a regional NW-SE orientation of the minimum horizontal stress. This stress direction is not compatible with the orientation of rift structures in the region, suggesting that this is a younger stress regime.

Introduction

Stress fields in the Earth's crust give us important information about past, current and future geologic events. Earthquake focal mechanisms and drilling are two of the most dominant sources of stress data worldwide (Figure 1). In Antarctica there are almost no stress data due to its near aseismicity and the lack of commercial drilling.

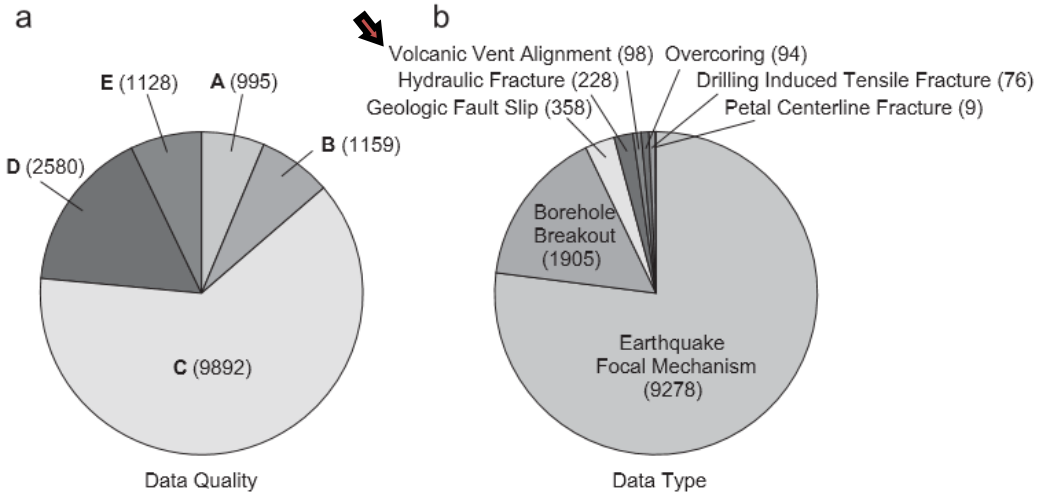

Figure 1. Statistics of World Stress Map 2005 database release. In brackets: number of data for each subset. (a) Quality distribution of 15,976 stress data records. More than 75% have A-C quality, i.e. horizontal stress (*S*H) orientation is reliable to within ±25º; (b) distribution of stress indicator type of 12,046 A-C quality stress data. Note the usage of volcanic vent alignment data [Modified from: Heidbach & Höhne 2008].

The widespread Cenozoic volcanic provinces of Antarctica provide an opportunity to use volcanic alignments as a means to map Cenozoic stress fields. Signatures of rifts, whether continental or marine, include normal faulting, fissures and extension fractures, and lineations formed by elongated cinder cones/volcanic vents (Figure 2). The mapping of linear arrangements of monogenetic volcanic vents allows for determination of the trend of stress and strain at the time the vents formed. Volcanic arrays form in platform volcanic fields due to separated

eruptions along the trend of fissures fed by subsurface feeder dikes [MacDonald, 1972; Settle, 1979]. Subsurface feeder dikes and their surface vents form alignments parallel to the maximum horizontal stress (S_H) in the upper crust due to magmatically-induced intrusions or by the exploitation of preexisting fractures oriented at a high angle to the minimum horizontal stress (S_h) [Anderson, 1951; Nakamura, 1977; Delaney et al., 1986]. By studying the morphometry and alignments of cinder cones one can define the trend of the underlying fissure, thus determining the horizontal stress directions at the time of the fissure eruption. The elongation direction of elliptical vents closely constrain the fissure orientation [Paulson & Wilson, 2010]. This research involves mapping volcanic vent alignments of a platform volcanic field on the seafloor of the northwestern Ross Sea, Antarctica.

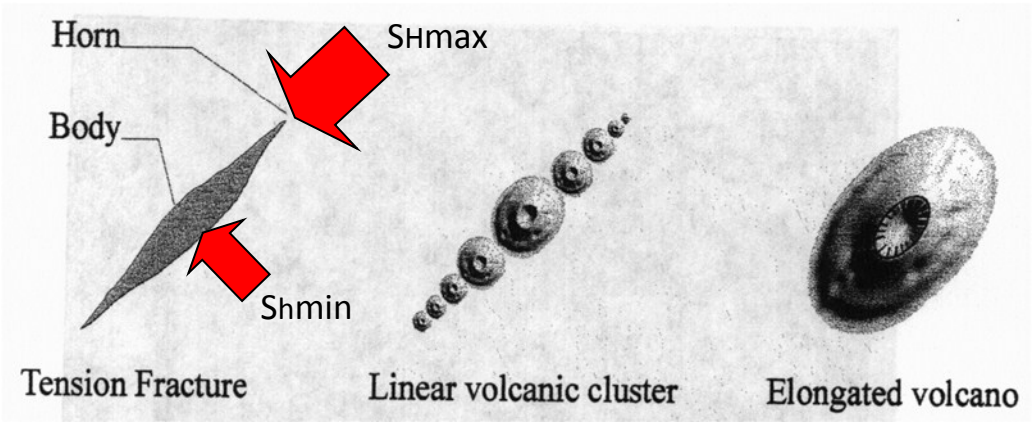

Figure 2. Surface signatures of volcanic fissures, and their stress directions. [Modified from: Adiyaman et al., 1998].

In the last few decades there has been a large amount of multibeam swath bathymetry data collected on the seafloors surrounding the continent of Antarctica from research vessels (Figure 3). The vessel used to acquire the data for this study, named the *RVIB Nathaniel B. Palmer*, cruises off the shore of Antarctica from New Zealand every year to collect sea floor data. Digital bathymetric survey data from near Cape Adare, Antarctica, on the Adare bight,

which I call the Southern Adare Volcanic Field or SAVF, are used in this study to characterize volcanic cone morphometry and map volcanic alignments. The trends of fissures defined by these alignments constrain the upper crustal stress directions. This study forms part of an ongoing project to map the stress patterns in the McMurdo Volcanic Province across the western Ross Sea. Results of this study make a worthy addition to the known Antarctic stress field and will contribute to the understanding of the crustal stresses of Antarctica.

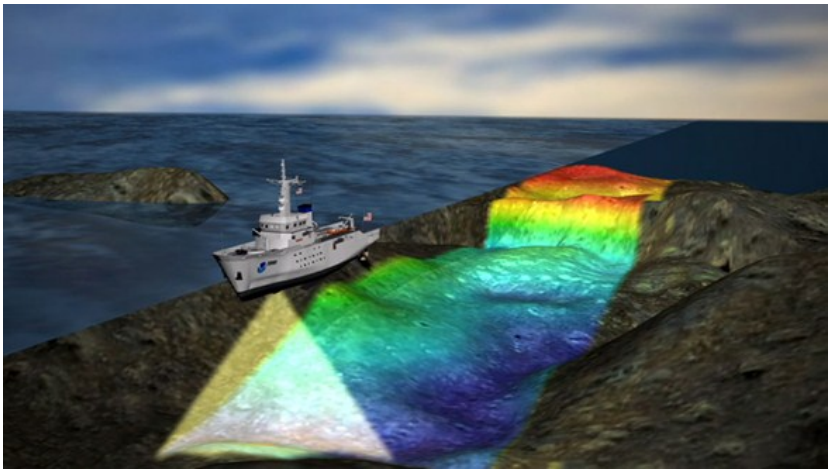

(Figure 3. Source: NOAA).

Geologic Setting

The Ross Sea lies within the West Antarctic Rift system (WARS). The WARS (Figure 4) represents one of the largest continental rifts found on Earth [LeMasurier, 1990]. A Rift is formed when the Earth's crust is pulled apart creating tensional forces in the region between the two spreading plates. These tensional forces produce faulting, and volcanic eruptions from the partial melting of the lithosphere (Figure 5). The WARS is marked by extensional faulting [Davey & Brancolini, 1995], widespread young (Cenozoic) volcanism [LeMasurier, 1990] and the uplift of the Transantarctic Mountains which separate West Antarctica from the more cratonic East Antarctica [Stern and ten Brink, 1989]. The total

continental extension (Cretaceous to Cenozoic) has been estimated to be from approximately 250 km [Fitzgerald et al., 1986; Behrendt and Cooper, 1991] to as much as 1000 km [Divenere et al., 1994].

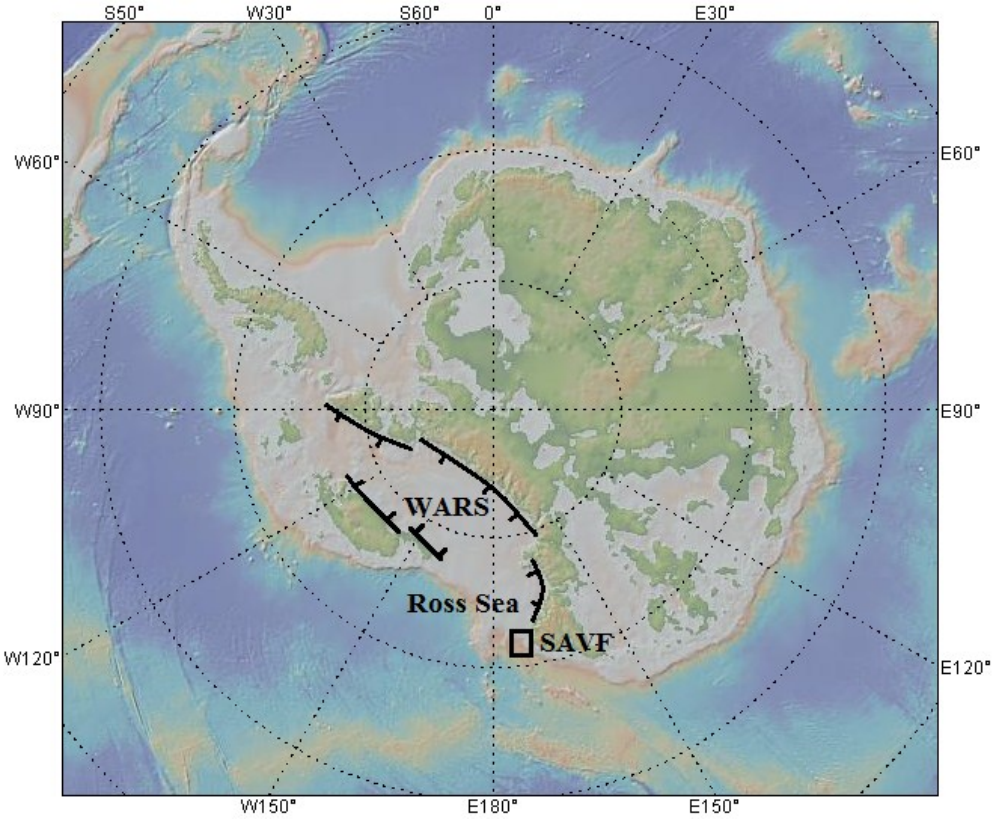

Figure 4. Map of Antarctica showing the West Antarctic Rift system (WARS) and the location of the Southern Adare Volcanic Field (SAVF). [Produced using GeoMapApp 3.3.0]

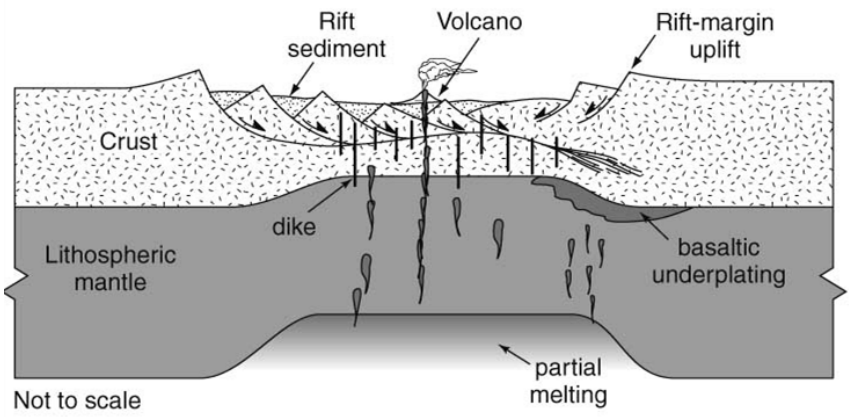

Figure 5. Profile view of an active rift system. [Van Der Pluijm & Marshak, 2004]

On the ocean floor of the north-western Ross Sea, geophysical markers such as marine magnetic anomalies have defined a period of seafloor spreading from around 43 – 26 Ma which formed the Adare basin where approximately 170 km of extension occurred trending ENE-WSW (Figure 6) [Cande et al., 2000; Cande & Stock, 2005; Granot et al., 2010].

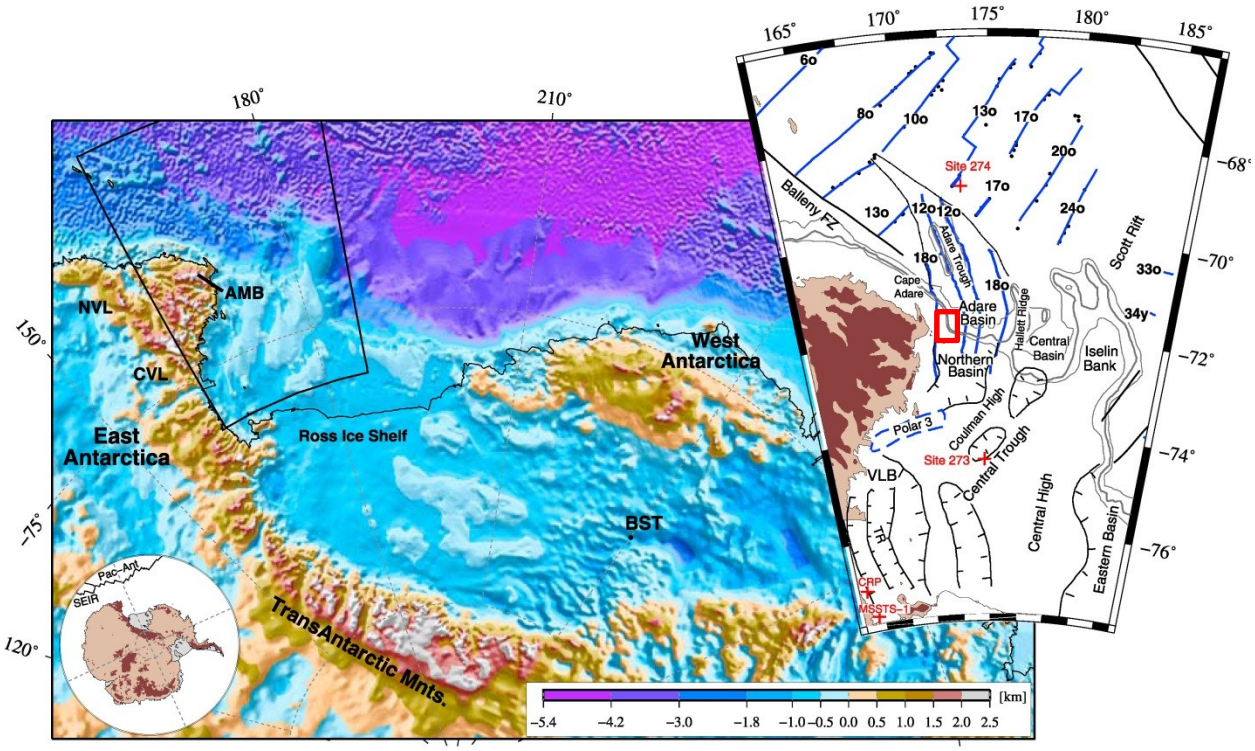

Figure 6. Tectonic setting and location map of the West Antarctic rift system. Large inset shows the main structural elements of the Adare Basin and western Ross Sea. Adare Bight (SAVF) boxed in red. Blue lines indicate magnetic lineations based on shipboard magnetic data and aeromagnetic data [Granot et al., 2010].

Granot's studies reveal evidence of rifting in the early Miocene (~17 Ma) which resulted in normal faulting of the Adare Basin (Figure 7). This caused the formation of the Adare Trough and marks the last true extensional phase of the Adare Basin. Young volcanic vents mapped by Granot (Pliocene and younger) tend to align with the early Miocene structures (NE-SW). Granot mapped with the use of seismic reflection data and bathymetric data with which he found

prominent volcanic activity and nearly vertical normal faults with insignificant horizontal effects on crustal movement in the Adare region (Figure 7).

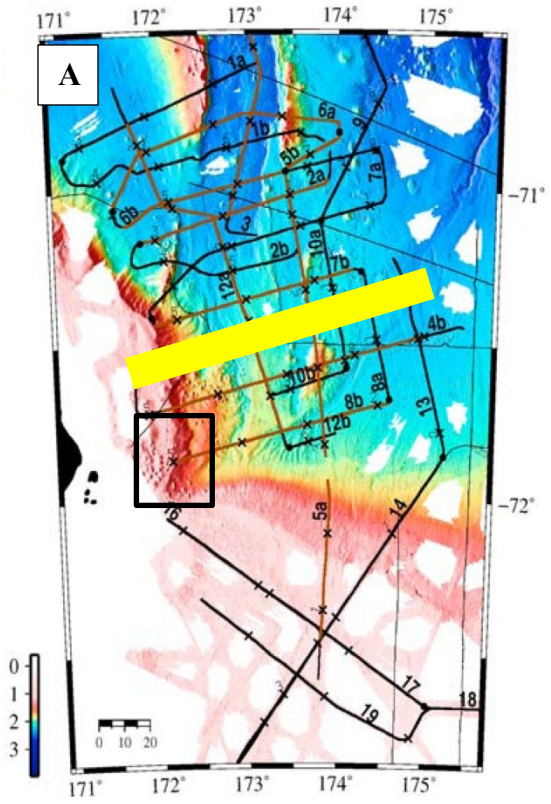

Figure 7. (a) Map of NBP0701 multi-channel seismic grid lines with SAVF boxed in black. (b) Seismic profile of line 4b (highlighted in fig. 7a) revealing near-vertical normal faults, volcanoes, channels and uplifted zones [Granot et al., 2010].

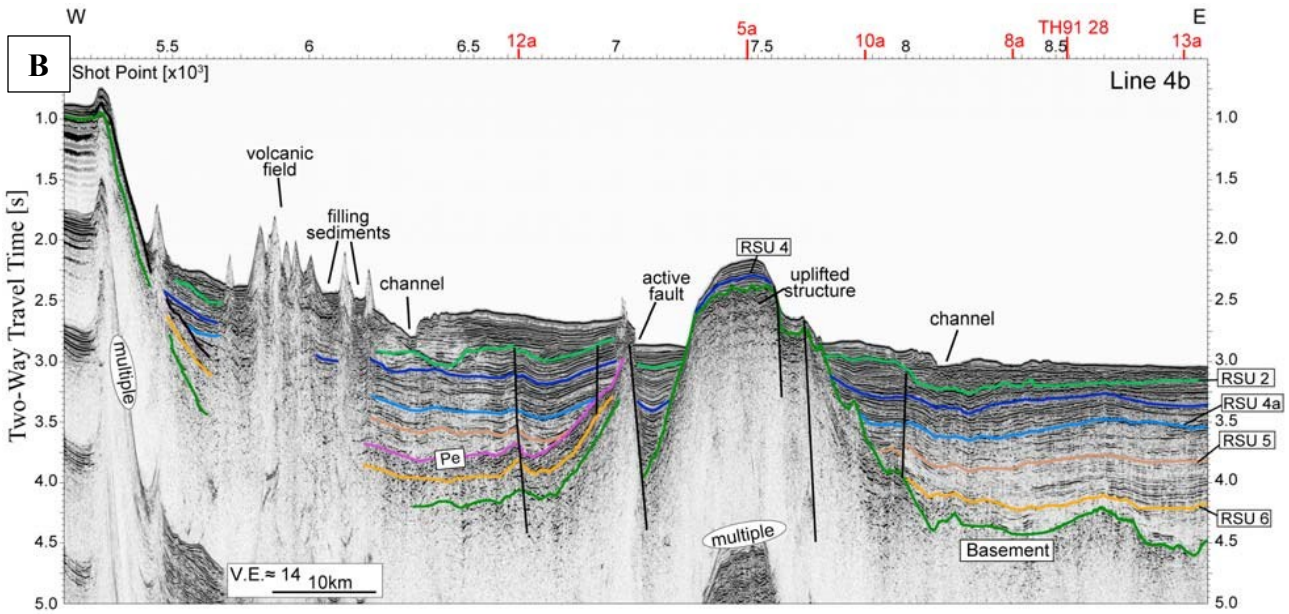

During the 2007 Nathaniel B. Palmer research cruise, 3 volcanic seamounts of the southern Adare volcanic field (SAVF: Figure 4) were dredged with high precision for isotopic ($^{40}Ar/^{39}Ar$) dating (Figure 8). The dredge log revealed basaltic samples with igneous and metamorphic dropstones released from melting ice bergs. The ages of the 3 basaltic seamounts were determined to be 0.32 ±0.23 Ma [Kurt Panter, personal communication, 2012] Alignments including these volcanic vents mark subsurface fissures formed around 320,000 years ago.

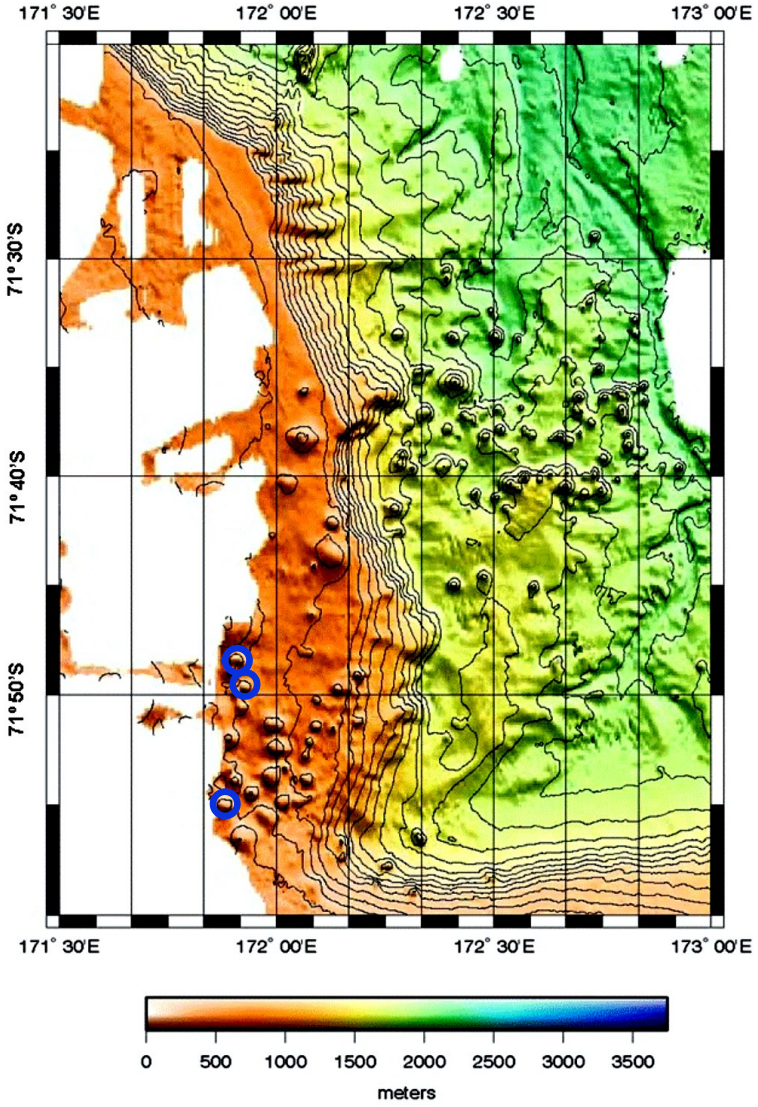

Figure 8. High precision dredging of 3 sea mounts (circled in blue) within the SAVF revealing ages of 0.32 ±0.23 Ma [Modified from: Kurt Panter, personal communication, 2012].

Methods

Determining Stress Directions from Volcanic Cone and Fissure Alignments

Volcanic processes which cause the fracturing of rocks are related to regional crustal stresses acting on volcanic regions [Nakamura, 1977]. The regional stresses influence the orientation of rifts, dikes, and volcanic vents, including seamounts [Nakamura, 1977]. Because magmatic dikes and fissures are opening-mode fractures, they are oriented perpendicular to the minimum horizontal stress, and parallel to the maximum horizontal stress [Anderson, 1951] (Figure 2). By mapping the distribution of volcanic seamounts, taking into account their orientation and morphometry, one can use their mapped orientations as an indicator for the average orientation of tectonic stresses in the upper crust at the time they formed. Monogenetic volcanoes erupt only once from a vent or fissure, constructing relatively small volcanic edifices such as scoria cones or maars. A set of small cones may form along a fissure, as the sheet of rising magma erupts preferentially in cones due to cooling, or, each volcanic edifice may be produced by a newly formed underground conduit or dike [Nakamura, 1977]. The trends of these volcanic edifices tend to be perpendicular to the stretching direction in continental rifts and parallel to the convergent plate motion direction in the magmatic arc above subduction zones [Nakamura, 1977].

Using Seafloor Multibeam Bathymetry Data to Map Volcanic Alignments

Bathymetry data: acquisition and processing

Bathymetry originally referred to the oceans depth relative to sea level, but today bathymetry has come to mean submarine topography (NOAA, 2013). Bathymetry is collected from research vessels such as the *RVIB Nathaniel B. Palmer,* which are equipped with a sonar

multibeam instrument, sound velocity sensors and thermosalinographs (TSG's). These three tools are used together to create topographic maps of the sea floor. Sound velocity sensors use the Doppler Effect to measure the speed of sound in the water, which changes with water temperature and salinity. This creates a need for a TSG, which is an automated system that measures the sea surface temperature and salinity by using a water intake. The sonar multibeam tool creates a swath of sound beams directed like a fan towards the sea floor, where the sound waves bounce back towards the ship, and the time it took for the sound to travel down and come back is measured (Figure 3). The data collected from the sound velocity sensors and TSG's is used to convert travel time to depth and determine the sea floor topography.

All of the bathymetric data acquired by the Palmer is archived in a component of the Marine Geoscience Data System (MGDS) called the Antarctic and Southern Ocean Data Portal [http://www.marine-geo.org/portals/antarctic/]. The MGDS provides the application GeoMapApp 3.3.0, which provides internet access to "a rich content of information for physical oceanography, paleoclimates, geochemistry, geology, seabed sediment and rock compositions, ocean crust age, spreading rates, bathymetry, and sediment thicknesses" [GeoMapApp.org]. For this study I downloaded the available bathymetric data sets for the Adare bight region of the western Ross Sea that had been acquired from the *Nathanial B. Palmer* (Figure 9). Figure 10 shows the track lines of where the Palmer has collected data over the last 12 years in the Ross Sea. Figure 11 shows a chart of all the files used in this study collected to produce topographic maps. Figure 12 shows all of the track lines of the *Nathanial B. Palmer* where bathymetric files/data was collected. Figure 13 shows the product of the files collected and the corresponding track lines overlain.

Figure 9. *RVIB Nathanial B. Palmer.*

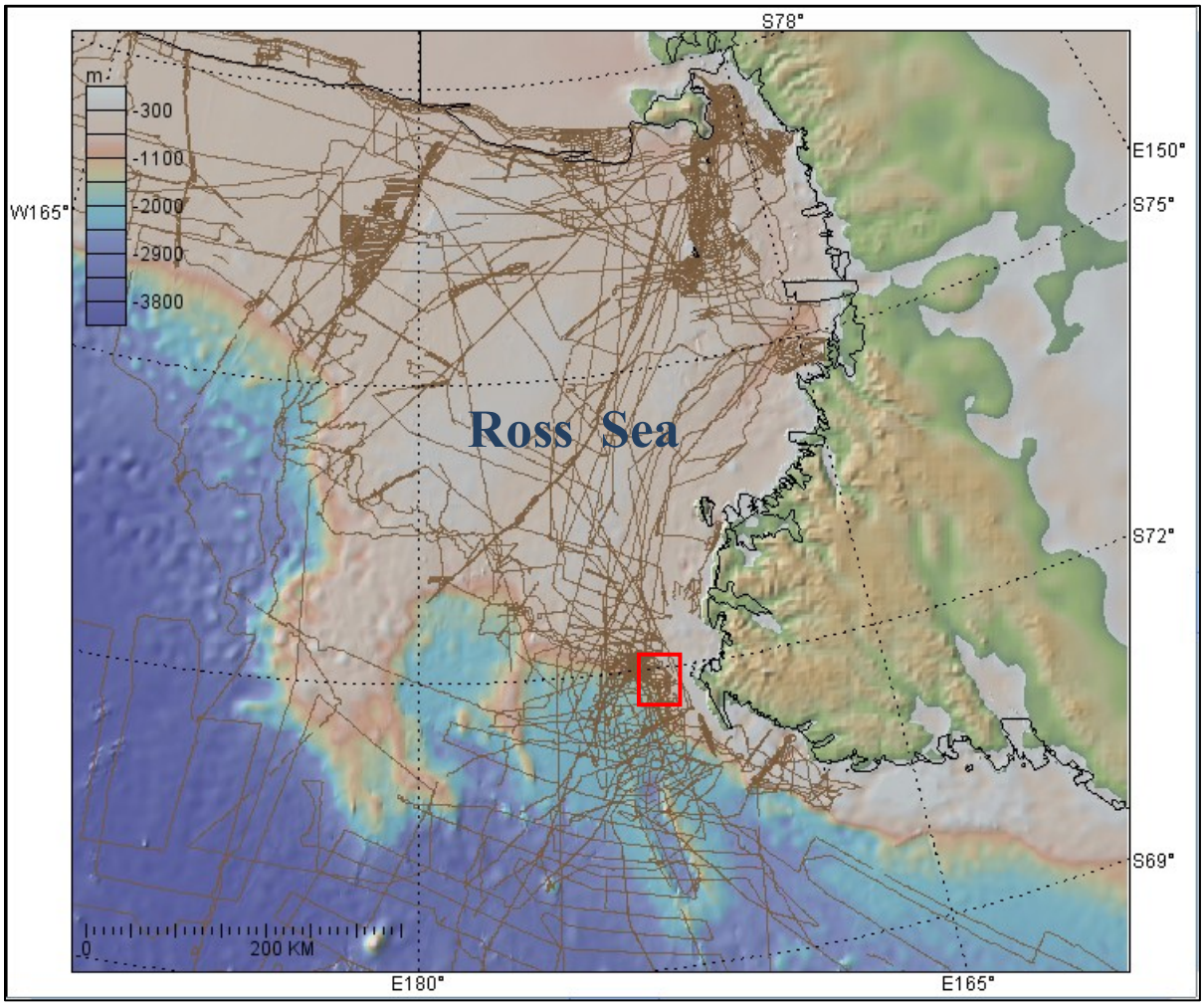

Figure 10. Track lines from the *Nathaniel B. Palmer* where areas of bathymetric data were collected (seen as brown lines). SAFV boxed in red. [Produced using GeoMapApp 3.3.0, 2012].

Bathymetric Files, Collected by the *Nathanial B. Palmer*				
NBP0209	NBP0302	NBP0402	NBP0701	NBP0801
0318	0130	0226	0538	0130
0319	0131	0227	0539	0131
0320	0132	0228	0540	0132
0321	0164	0231	0541	
0326	0165	0232	0542	
0327	0169	0234	0543	
0330	0170	0235	0544	
0331	0171	0236	0545	
0364	0172	0243	0548	
0365	0173	0244	0551	
0366	0174	0245	0553	
0367	0175	0246	0554	
0373	0176	0247	0846	
0374	0177	0248	0847	
0375	0178	0250	0848	
0376	0179	0251	0849	
	0180	0264		
	0181	0265		
	0182	0303		
	0184			
	0185			
	0186			
	0194			
	0226			
	0226			
	0227			
	0227			
	0228			
	0231			
	0232			
	0233			
	0234			
	0235			
	0235			
	0237			
	0239			
	0625			
	0627			
	0629			

Figure 11. List of all the files used in this study from 5 different cruise years of the *Nathanial B. Palmer*. (Files uploaded from Antarctic and Southern Ocean Data Portal).

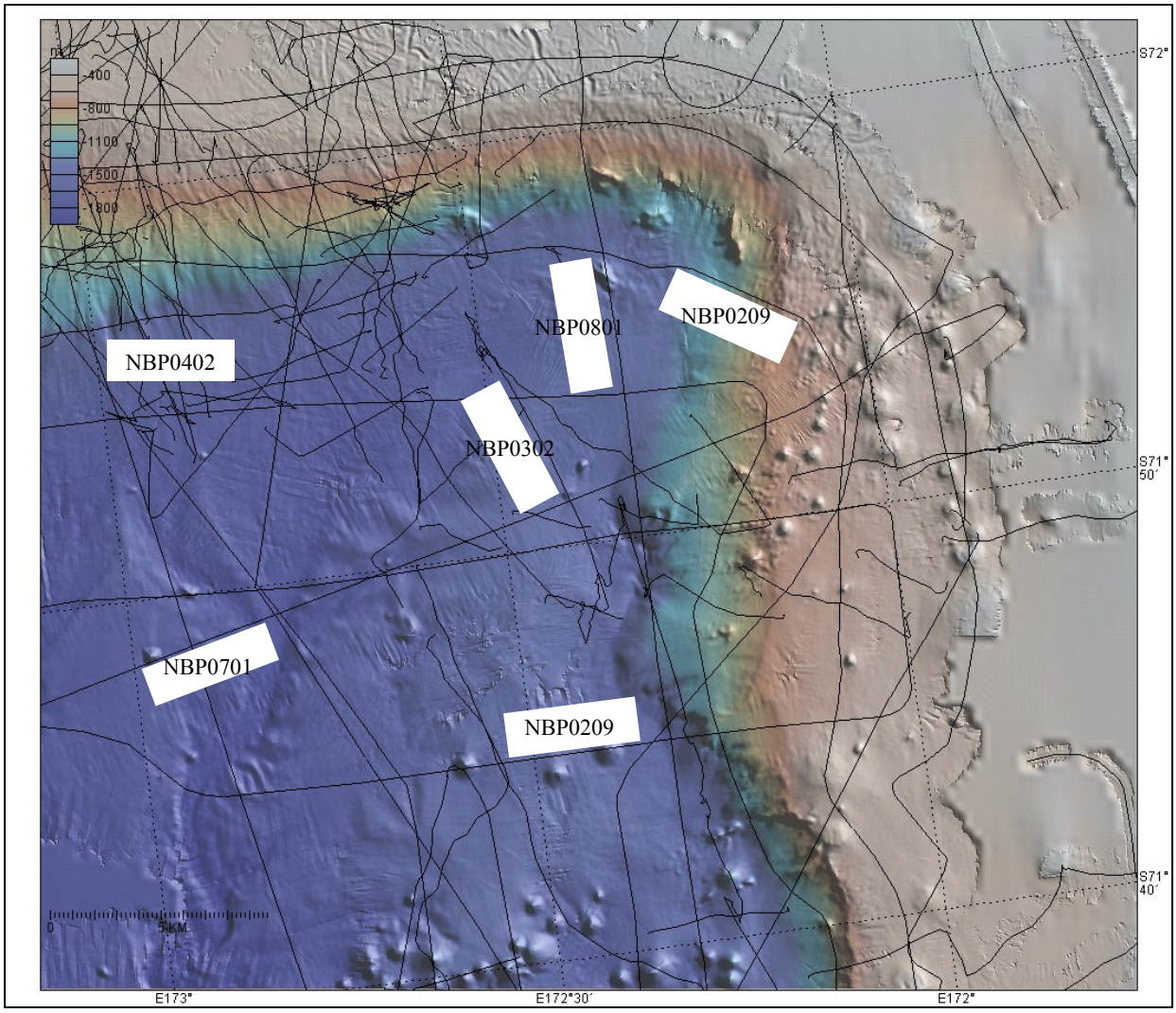

Figure 12. Track lines where multibeam bathymetric data was collected in the Adare bight by the 5 research cruises used for this study. [Produced using GeoMapApp 3.3.0].

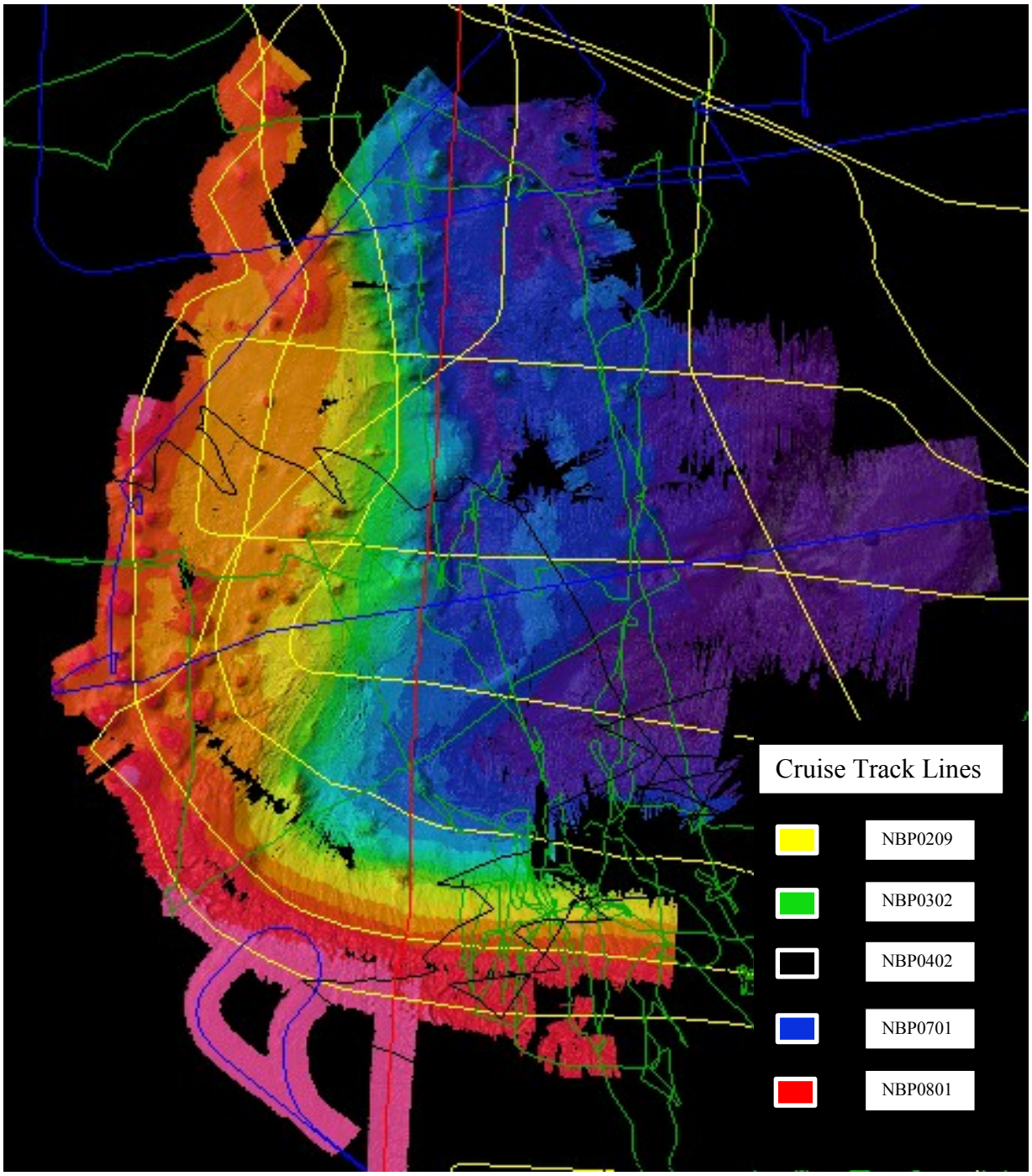

Figure 13. Aerial map view of SAVF with track lines of the Nathanial B. Palmer where multibeam bathymetric data was collected, color corresponds to cruise year. Produced in Fledermaus.

The bathymetric data was downloaded in MBSystems format which is a data format read only by MBSystems, an open source bathymetric data software package, maintained and serviced by the Monterey Bay Aquarium Research Institute and Lamont-Doherty Earth Observatory [http://www.mbari.org/data/mbsystem/html/mbsystem_home.html]. The data was converted from MBSystems format to standard ASCII (XYZ) format. The data sets were then transferred into Fledermaus for viewing and further processing. Fledermaus is an interactive 3D geo-spatial analysis tool [http://www.qps.nl/display/fledermaus/main]. There were significant data quality problems, which required editing. I then had to reprocess some of the data files by deleting the extraneous data using 3D Editor which allows the user to make data edits within Fledermaus. Fledermaus allows you to select a location on the map which when you open 3D Editor shows the selected location as a 3D map represented by the cubes/bins which coalesce together to represent that selected location (Figure 14). Within 3D Editor the user can then selectively choose the cubes deemed as noise or as unnecessary data (Figure 15).

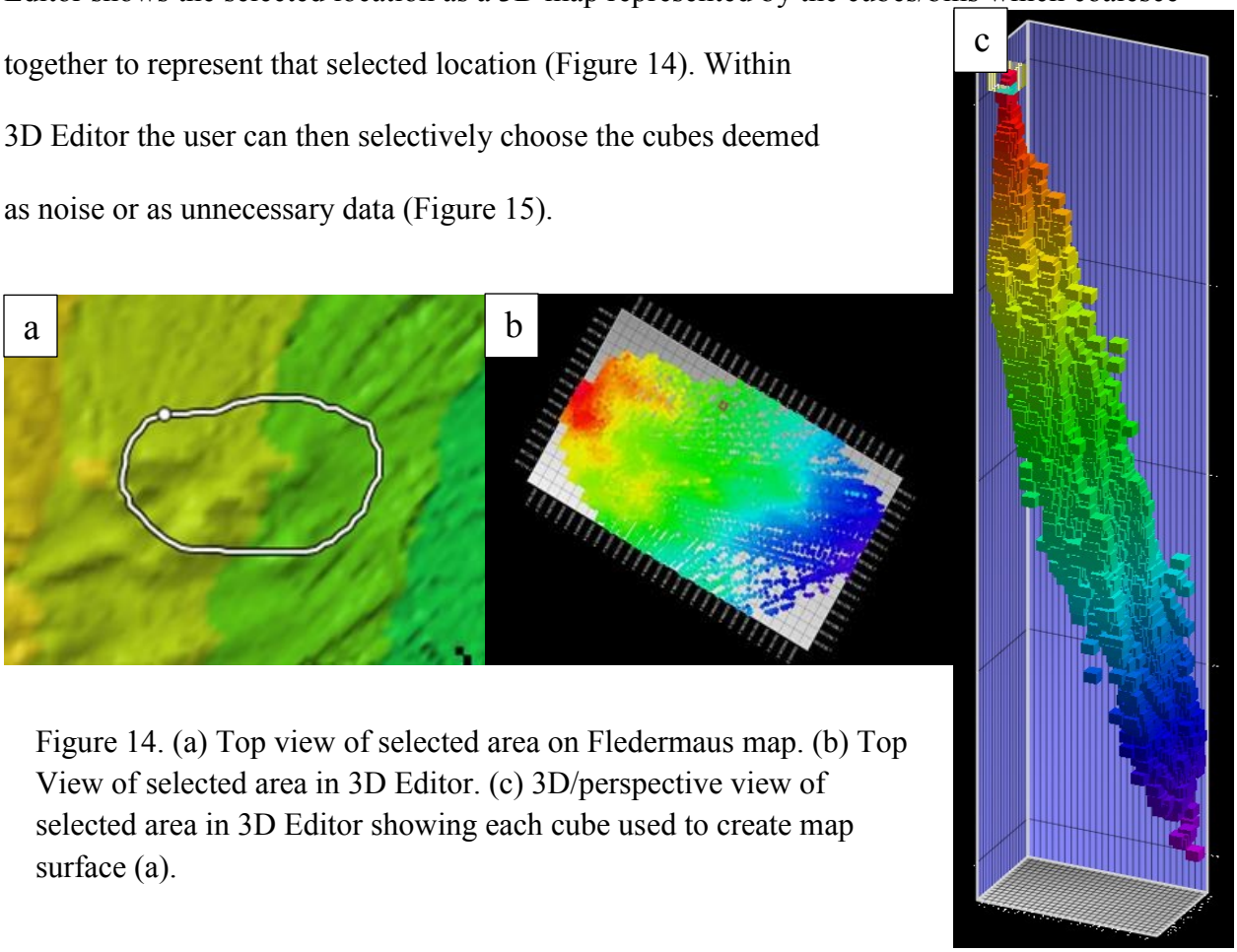

Figure 14. (a) Top view of selected area on Fledermaus map. (b) Top View of selected area in 3D Editor. (c) 3D/perspective view of selected area in 3D Editor showing each cube used to create map surface (a).

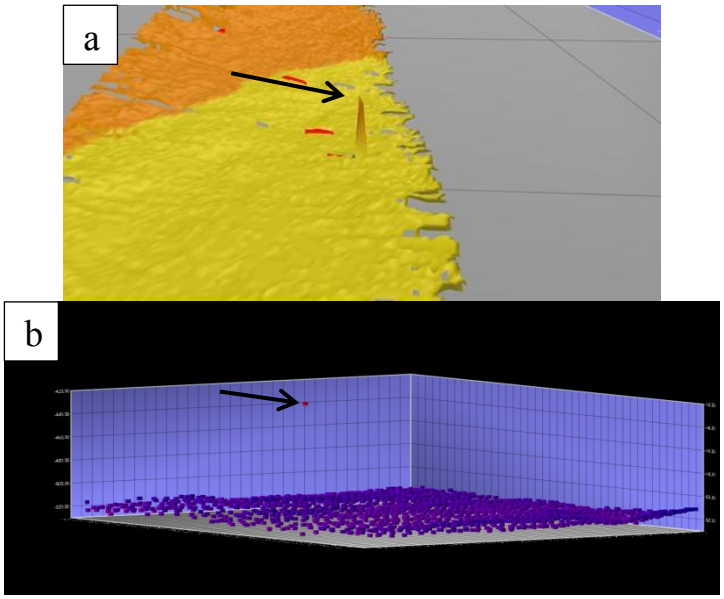

Figure 15. Data feature deemed as noise. Seen as Fledermaus perspective view (a), and 3D Editor perspective view (b). Red dot in figure (b) represents the error causing the spike in figure (a).

Most of the data that I had to delete was either from locations not pertaining to the specific study area or from tracks with poor data quality. The bad data could be a direct result of the ship moving too fast for the sonar instrument to be able to collect a complete surface image (Figure 16a) and/or from major changes in the pitch, roll, yaw or heave of the ship (Figure 16b) in rough seas, causing the swath to twist and become extended with unequal spacing between collected data (Figure 16c). A Complete edited map is seen in Figure 17.

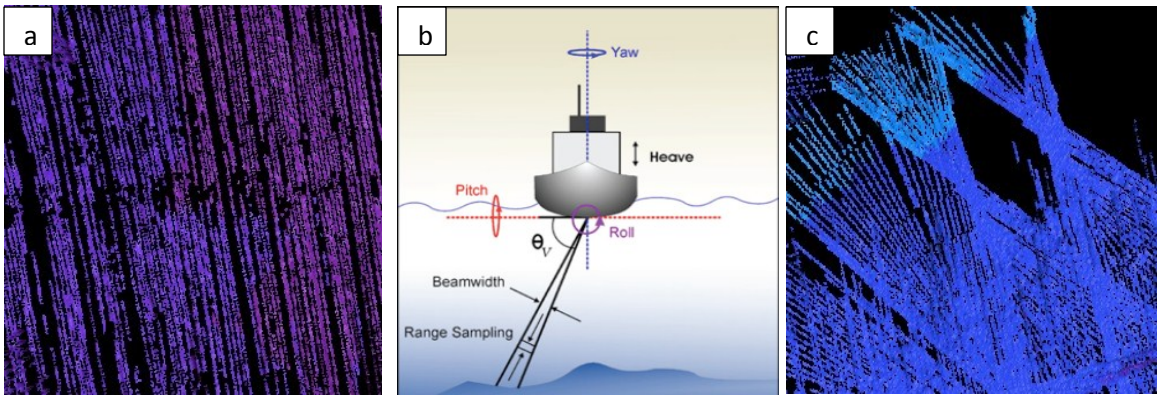

Figure 16. (a) Multibeam track line resulting from ship velocity exceeding capability of multibeam system to image seafloor; (b) illustration of ship movements that can produce erroneous seafloor depth measurements [D. Mallace, www.ivs3d.com]; (c) Multibeam track line produced when ship movement in rough seas causes the ship to twist off course and change velocity.

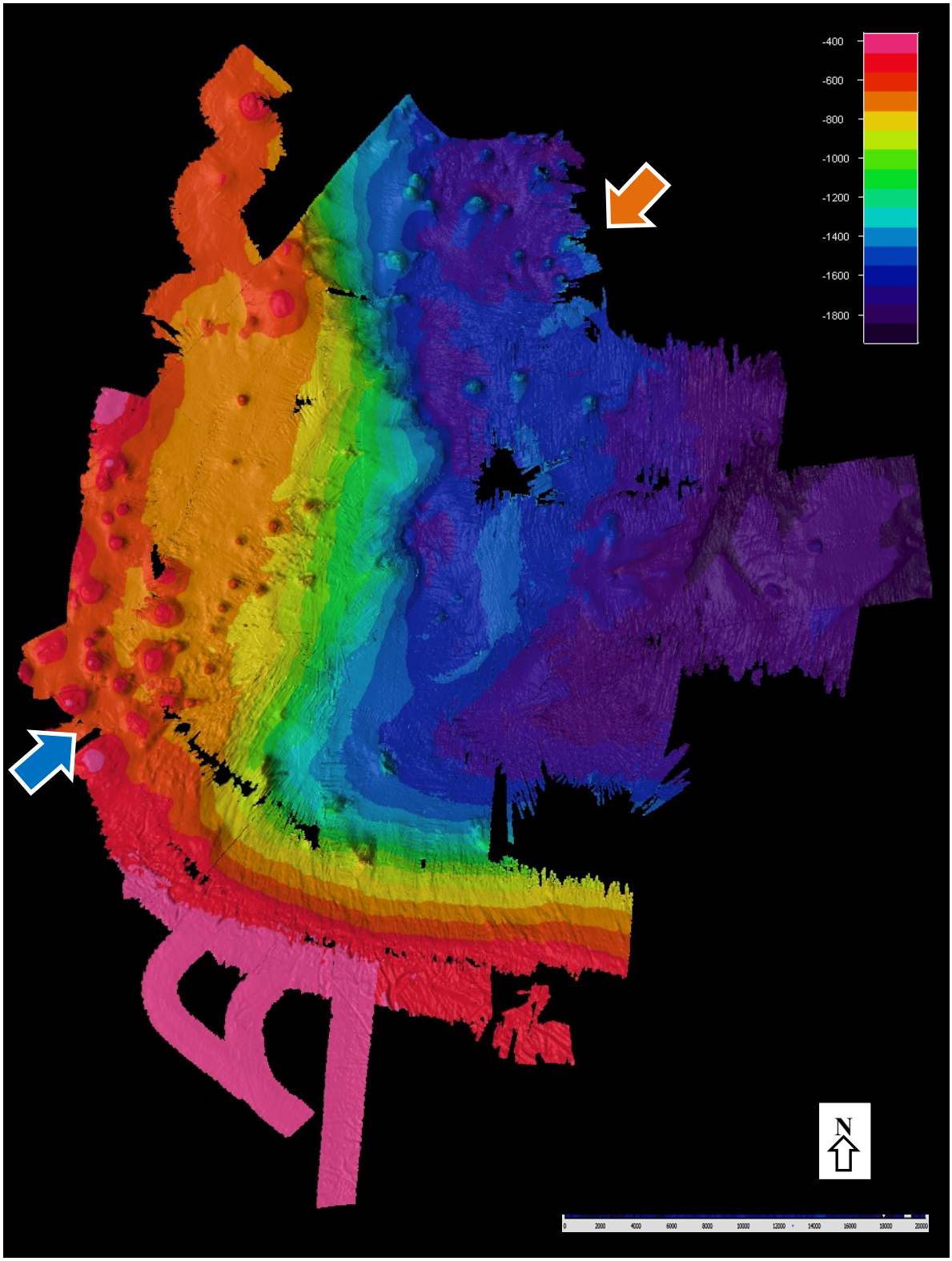

Figure 17. Aerial view of edited SAVF map produced in Fledermaus showing cones as locations with elevated relief from their surroundings. Blue and Orange arrows revealing view points for figures 18 & 19. (Color scale based on depth, both scales in meters).

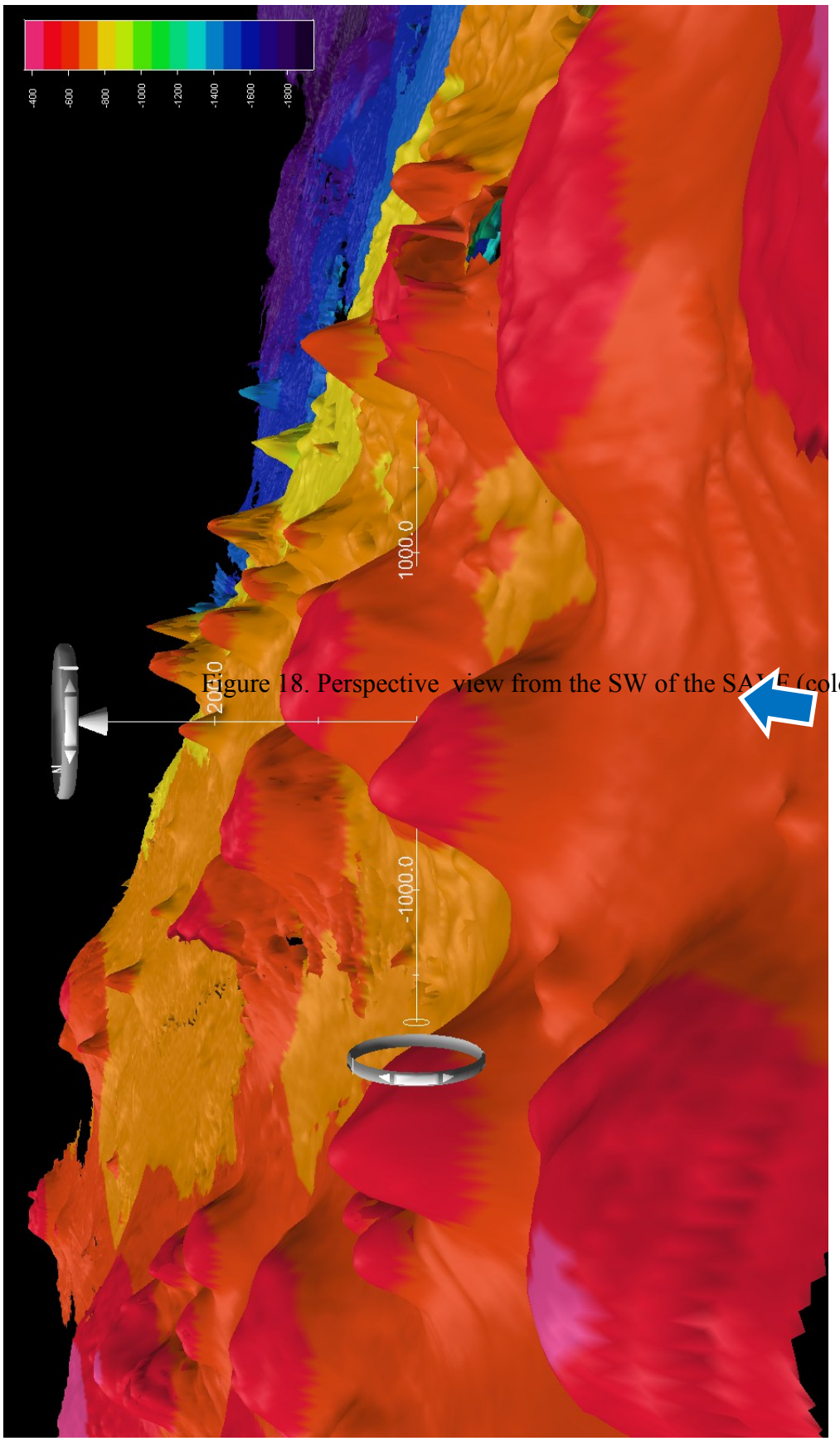

Figure 18. Perspective view from the SW of the SA[illegible]F (color scale based on depth, bo

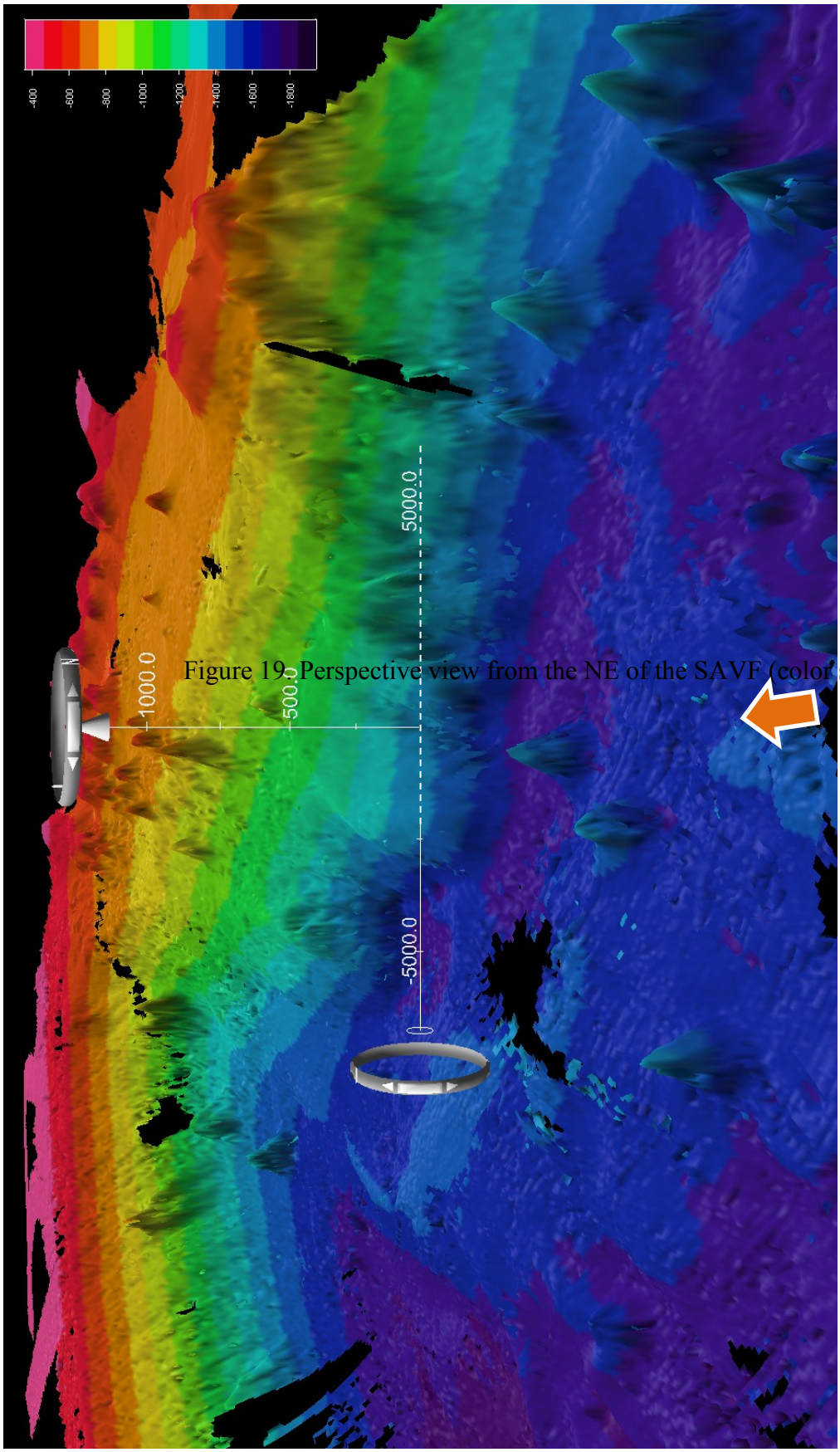

Figure 19. Perspective view from the NE of the SAVF (color scale based on depth, both

Due to missing data, or poor data quality, it was necessary to create different bin size grids for the seafloor depth data in different parts of the study area. A 'bin size' is the grid point spacing in meters which can be changed as needed within the Fledermaus PFM files, which are file structures used for surface visualization, but which also allow for the editing of that surface. I started each PFM with a bin size of 20m in order to try and preserve as much detailed topography as possible. However, one area required regridding to a bin size of 40 m and a second area required a bin size of 80 m to mask data quality problems.

Fledermaus and ArcGIS: Image Enhancement and Tools for Mapping

When satisfied with my reprocessed Fledermaus data set, I transferred it to the program ArcGIS10 to and projected it using the following coordinate system:

Lambert Conformal Conic

0.0º false easting

0.0º false northing

central meridian of 172.166667º

latitude of origin of -71.791667º

linear units in meters

Within ArcGIS I used the slope and hillshade tools to create maps that more clearly show the regional morphology, including the seamounts and their shapes. The slope spatial analyst tool identifies the slope/gradient between cells of a raster surface and creates maps with color-coded slope angle or percent rise (Figure 20a). The hillshade spatial analyst tool creates a shaded relief from a surface raster by applying a designated illumination source angle and direction, which creates shadows that highlight features perpendicular to the false illumination direction (Figures 20b & 21). To define the break in slope that outlines the base of each volcanic cone, I examined

the slope histogram and found that the typical break in slope for cone bases is within the range of 6-9%. In Arc a flat surface is given a 0 percent rise and a 45° surface is given a 100 percent rise so 6-9% is 3.4° to 5.1° degree slope. To better define the break in slope at each cone I introduced contrasting colors above and below the slope break angle to make it stand out. This gave a color stretch which more accurately showed the base of the cones. I then created an aspect map layer in ArcGIS which I laid over the slope map and gave a 60% transparency to be able see the underlying slope map with a visualization of the aspect map. Using the newly made slope/aspect raster map (with a custom color stretch), I used a polygon tool to map the base of each volcano. After mapping each volcanic seamount base with a polygon tool in ArcGIS, I fitted a circle or ellipse to the shape. For elongate cones, the dimensions and orientations of the long and short axes of each seamount were measured in Arc to determine the index of elongation (Figure 22b).

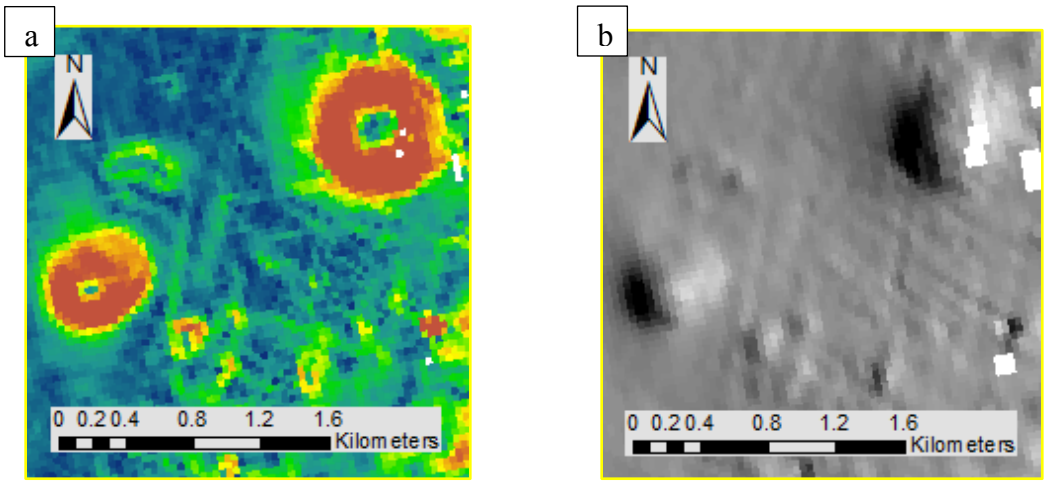

Figure 20. (a) Slope and (b) hillshade map close-ups. Produced in ArcGIS.

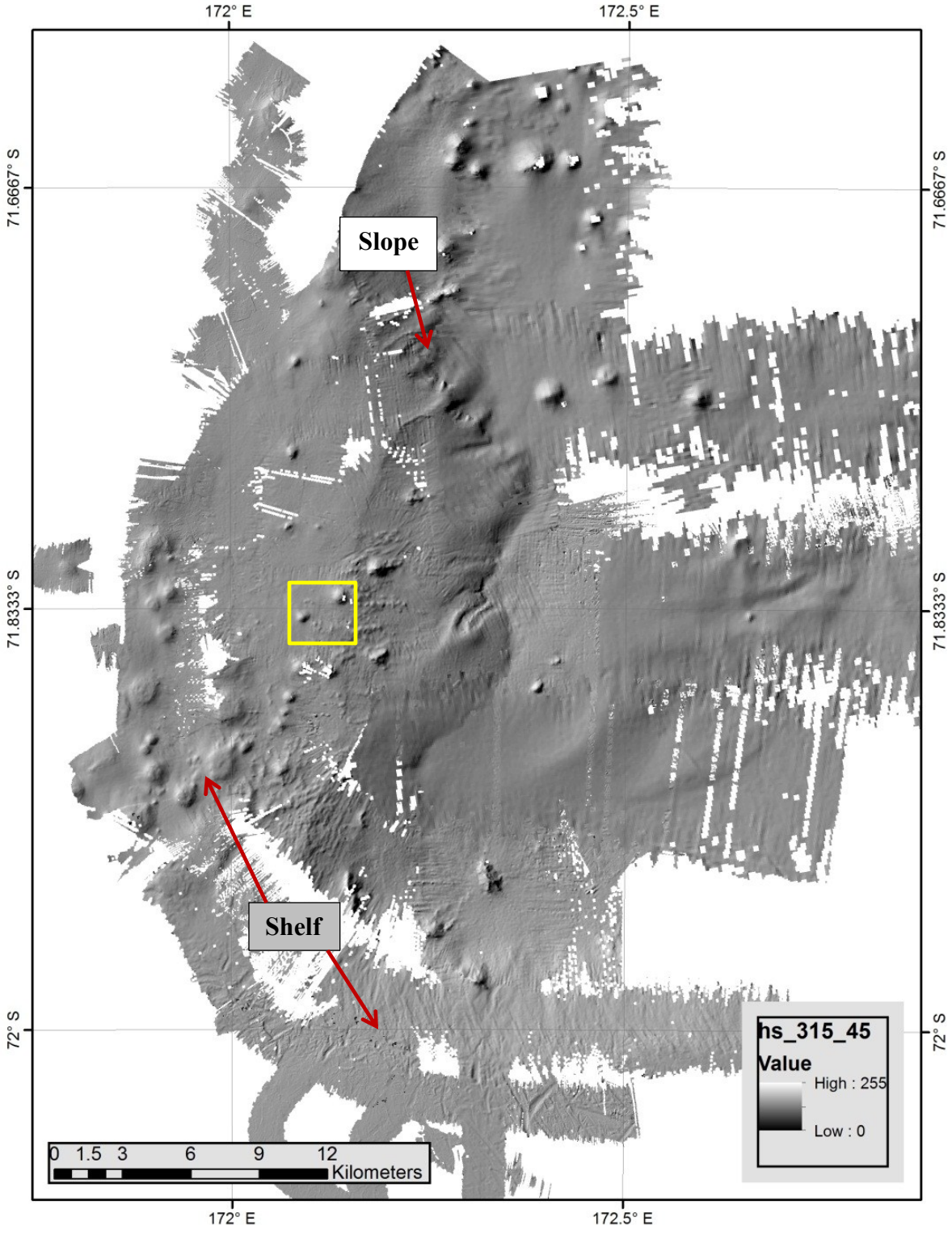

Figure 21. Hillshade map showing boxed location of area for 20a and 20b, slope and shelf of SAVF.

Selecting Alignments and Testing Alignment Reliability

The Paulson & Wilson (2010) method was used for defining alignments and their alignment quality (Table 1). The regional subsurface dike trend is best constrained where elongated vents align with proximal elongate or circular vents of a similar age and composition [Paulson & Wilson 2010]. Vent alignments were drawn with the polyline tool in Arc, based on clusters of cones close to each other and guided by cone elongation. The azimuth of each alignment was then measured. The Paulsen and Wilson (2010) method allocates individual alignments into four reliability grades (A>B>C>D). Their method is based on the following alignment characteristics: numbers of vents, standard deviations of vent centers from a best fit line by an orthogonal regression, evaluation of elongate vents / index of elongation (number of elongate vents and their axial ratio), standard deviations of the trend of elongate vent long axes from the trend of a best fit line, and average vent spacing distances (Figure 22). Higher grades (≥B) represent a higher confidence that an alignment signifies a subsurface feeder dike while lower grades (≤C) represent a lower confidence but could still signify a possible dike trend.

Reliability grade	# vents	Standard deviation best-fit line distance (m)	Index of vent elongation	Standard angular deviation vent long axes (°)	Average vent spacing distance (m)
A	≥4	≤125	1 cleft cone -or- 1 fissure ridge -or- 2≥1.6 -or- 1≥1.6 and 1≥1.4	≤30	No limit
	≥5	≤100	No shape data	No shape data	≤600[a] or ≤800[b]
B	≥3	≤150	1≥1.6 -or- 2≥1.4 -or- 1≥1.5 and 2≥1.2	≤35	No limit
	≥4	≤125	No shape data	No shape data	≤600[a] or ≤800[b]
C	≥2	≤175	1≥1.4 -or- 2≥1.2	≤40	No limit
	≥3	≤150	No shape data	No shape data	≤800[a] or ≤1000[b]
D	≥2	>175	1≥1.2	>40	No limit
	≥3	>150	No shape data	No shape data	>800[a] or >1000[b]

Table 1. Reliability assessment system for vent alignments. [Paulson & Wilson 2010] see Figure 22 for parameter definitions.

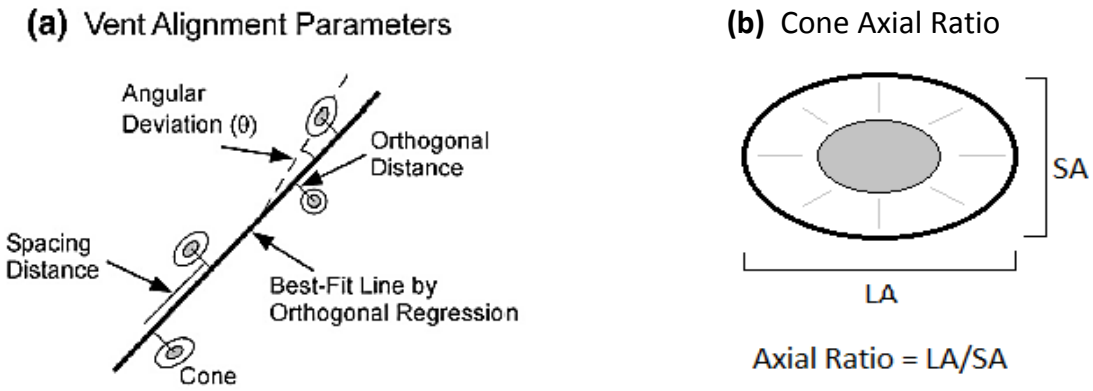

Figure 22. Attributes used for characterization and assessment of vent shapes and alignments. (a) The orthogonal distances of the vent center points from the best-fit line, the angular deviation of elongate vent long axes from the trend of the best-fit line, and the spacing distance between vents are used along with the types and numbers of elongate vents (i.e., the elongation index) to assess the reliability of individual alignments (Table 1). The best-fit line for an alignment is calculated by minimizing the orthogonal distances from points to the line (i.e., orthogonal linear regression). The angular deviation of fissure ridges, cleft cones, and elongate vents from the best-fit line is measured as the acute angle separating the long axis of the elongate vent and the best-fit line. Vent spacing distance is defined as the distance that separates adjacent vents found along the trace of the best-fit line. (b) The axial ratio of an elongate vent is the long axis length divided by the short axis length of the cone base. LA: long axis; SA: short axis [Modified from Paulson & Wilson 2010].

To determine the orthogonal distances from a best fit line I used EasyCalculate version 10 to determine the X/Y coordinates (in meters) of each volcanic center point. EasyCalculate is an ArcGIS add-in tool which calculates geometric characteristics of features produced in Arc. With the vent center point coordinates, I used a Deming orthogonal linear regression to mathematically show the best fit line through the cone centers. To computationally do the Deming orthogonal regression I used a software package called GraphPad Prism 6, which combines scientific graphing, comprehensive curve fitting, statistics and data organization for the analysis of scientific data [GraphPad Prism 6.00]. Regression results included an array of parameters such as X/Y intercepts, slope and Sy.x, which I used to calculate the best fit alignment azimuths and orthogonal distances from the best fit line to each cone center. Using the EasyCalculate tool in ArcGIS I determined the azimuths of the long axes of each cone to

determine the angular deviation from the corresponding best fit alignment (Figure 22a). Using these calculations I produced Table 2 showing all of the morphometric parameters for each of the 16 alignments.

Results

Improved Mapping with Digital Bathymetry

Enhanced Image Types

A large number of different raster maps, with different color scales, were created and evaluated. The hillshade (Figure 21), and hillshade overlain by a slope map (Figure 27), proved most useful for visualizing the overall morphology of the Adare bight seafloor. The break in slope defining the base of each seamount was well defined by the slope map when a custom color stretch was applied to highlight the steepening slope between ~ 3-5^{o}. The stretched slope map (percent rise) combined with a slope aspect map proved to be the best product for mapping cone shapes and alignments (Figure 27).

Morphologic Provinces of the Adare Bight

Very distinct morphologic areas are clear on the enhanced image maps created for cone mapping. At shelf water depths of ~400-600 mbsl, I found an abundance of iceberg scours with random orientations (Figure 23a). Slopes facing eastward and northward are characterized by gullies cut into the slope (Figure 24). Low-relief depositional lobes and channels occur on the deep seafloor, trending northeast from the corner of the bight, showing sediment transport offshore (Figure 25). Along the upper slope, just below the shelf-slope break, I found arrays of

small mounds resembling debris-avalanche deposits formed by volcanic eruptions or, possibly, some other type of landslide deposits (figure 23b).

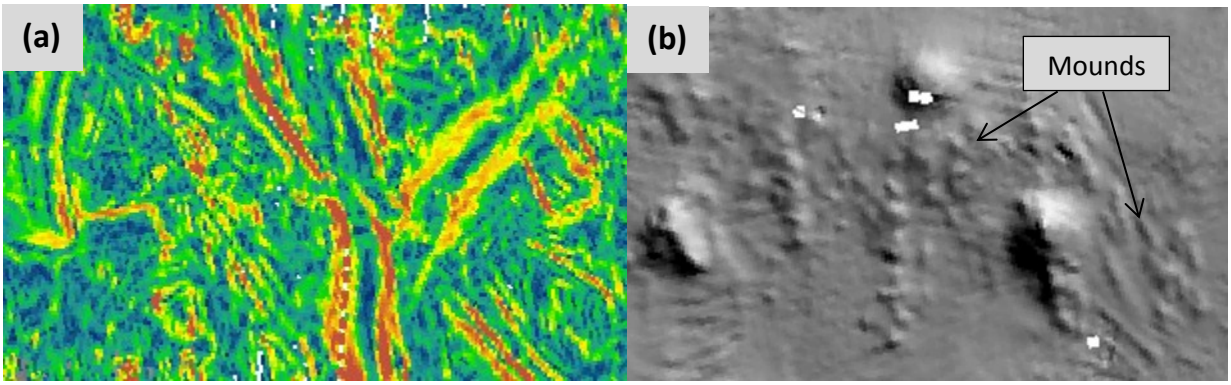

Figure 23. (a) Iceberg scours on the Southern shelf. (b) Randomly oriented and lineated mounds.

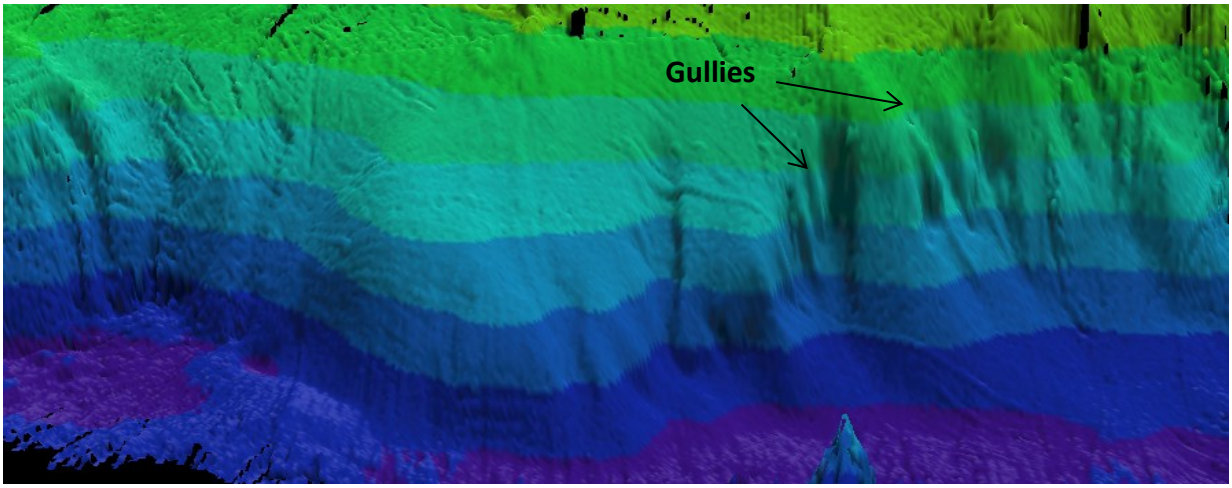

Figure 24. Oblique view of the slope of Adare bight showing gullies.

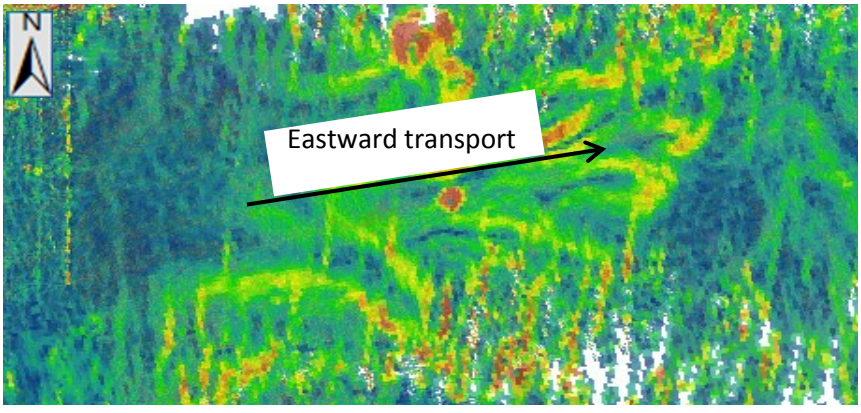

Figure 25. Slope map showing depositional lobes and channels with sediment transport moving eastward.

Seamount Morphology

Most cones in the volcanic field appear to lack craters on their summits. This could be the result of the lack of resolution in my data set or this could be the actual cone morphology. Many of the cones, all located at the more shallow, shelf depths, have very flat tops, resembling tuyas or table mountains (Figure 26). Tuyas are formed by volcanic eruptions under ice, with pillow basalt revealing evidence of quenching from the interaction of magma and the melted ice overlain by horizontal basaltic layering, forming the flat tops. The location of the flat-topped seamounts on the shelf approximately 67 km northeast of Cape Hallet and 45 km east of the Transantarctic Mountains, suggests they could be table mountains related to the advance of grounded ice sheet out on to the continental shelf. Alternatively, the flat tops could represent glacial erosion, with the tops planed off by glaciers. The well-developed U-shaped valley between the seamounts shown in figure 26 supports the idea that their shapes are related to glaciation. If they are in fact tuyas, then we can infer that the ice covered and extended down to the Southern Adare Volcanic Field at least 320,000 years ago. If the flat topped volcanoes have been planed off, then we can infer that the glaciers extended past the SAVF more recently than 320,000 years ago.

(a)

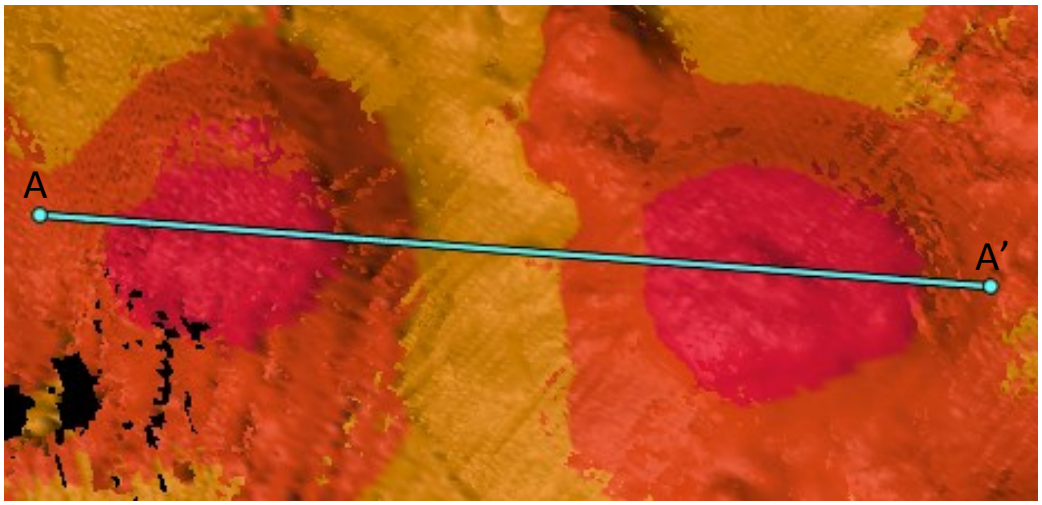

(b)

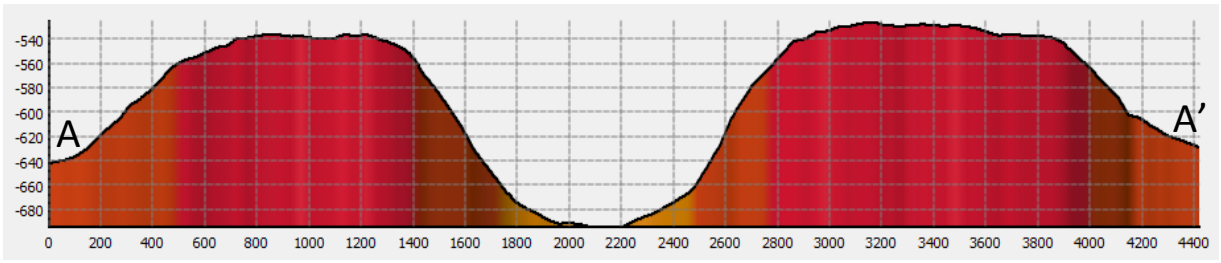

Figure 26. (a) Aerial view of 2 flat topped volcanoes; (b) Profile view of 2 flat topped volcanoes showing a near perfect U-shaped valley possibly carved out glacially (scale in meters).

Volcanic Alignment Trends

The results of the mapping of volcanic cone shapes and alignments are shown in figures 28-30. I identified and mapped 88 vents, 78% of which are elongate; 7 are possible fissure ridges, and 61 are elongate cones. These elongate cones and ridges trend predominantly NE-SW. I selected 16 alignments. The average azimuth of all the alignments is 054º, and the range of alignment azimuths is 005º to 133º.

The assessment of the reliability of vent alignment and morphometric data is necessary to evaluate the level of confidence that an alignment represents a subsurface dike. I used the method suggested by Paulsen & Wilson (2010) to produce Table 2. According to the reliability ranking suggested by Paulsen and Wilson (2010), the alignments I mapped have low grades. The two biggest factors in this assessment are the large spacing between cones along the alignments and the large orthogonal distances of the vents away from the best-fit lines used to define the alignments. An important point is that these seamounts are larger in overall dimensions than the scoria cones used by Paulsen and Wilson to define alignment parameters. Larger vents will always have longer distances between center points than smaller cones. Many alignments have relatively low values for the angular deviation of cone long axes from the

alignment azimuth, but others have high deviations. High angular deviations of vent long axes from the best fit alignment trends could be due to mapping lava flows radiating from the vent as part of the vent shape, creating an elongation different than the true vent shape. Flowing lava chooses a path of least resistance which will not necessarily be along the trend of the fissure. Erupted lava will flow down slope by the force of gravity, if a cone was formed on slopes like the Adare bight, the flowing lava will make its way down slope, not along the trend of the fissure/dike which fed the cone. This could be one problem with using the base of cones to map cone shape, although mapping cone bases provides a consistent mapping method.

Granot et al. (2010) mapped volcanic outcrops on the seafloor around the Adare Trough, which show a dominant NW-SE orientation. Rifting along this NW-SE trend is interpreted to be approximately 17Ma [Granot et al., 2010]. So the minimum horizontal upper crustal stress direction of the Adare trough at 17 Ma is NE-SW. The alignments of seamounts mapped in this study in the SAVF show a NE-SW trend. Using the age and composition data of 3 dredged cones provided by Kurt Panter, I have hypothesized that each cone within proximity to the 3 sampled cones are the same Pleistocene age of 0.32Myr. Since the cone alignments which I mapped show a strong parallel arrangement, I can infer that they were formed by the same upper crustal stresses and probably formed at close to the same time. Therefore the seamount alignments document a new minimum horizontal stress direction of Pleistocene age trending NW-SE (Figure 31).

Morphometric parameters of monogenetic cone alignments.									
Alignment #	Rock Type	Length (Km)	# Vents	Axial Ratios of Elongate Vents ≥ 1.10	Alignment Az (°)	SD of orthogonal distance from best fit line (m)	Angular Deviation vent long axis from best fit (°)	Avg. Vent Spacing Distance (Km)	Avg. Vent Long Axis Az (°)
1	B(a)	5.7	2	1.73, 1.59	007	N/A	9.2	3.4	050
2	B(a)	18	6	1.15, 1.26, 1.23, 1.17, 1.73	055	245.7	5.4	3.4	077
3	B(a)	7	4	1.61, 1.61, 1.11	076	181.2	4.1	1.9	074
4	B(a)	17.4	6	1.5, 1.26, 1.43, 1.35, 1.39	060	417.7	9.6	3.1	069
5	B(a)	12.1	3	1.25, 1.57, 1.41	055	354.1	11.4	5.4	064
6	B	9.3	6	1.61, 1.51, 1.22, 1.43, 1.49, 1.24	055	198.7	13.5	2.8	078
7	B(a)	4.9	2	1.62, 1.54	133	N/A	12.7	2.6	098
8	B(a)	8.6	3	1.23, 1.18	087	673.5	27.6	3.2	101
9	B(a)	4.7	4	1.43, 1.81, 1.81	021	348.9	12.9	1.1	054
10	B(a)	8.5	5	1.38, 1.63, 1.48, 1.29	048	483.7	19.5	1.6	076
11	B(a)	8.5	5	1.21, 1.67, 1.25	062	360.3	8.8	1.8	084
12	B(a)	19.3	8	2.42, 2.95, 1.11, 1.11, 1.88	066	433.9	6.2	2.6	064
13	B(a)	8.9	7	1.23, 1.43, 1.20, 1.69, 1.24	053	555.4	15.7	1.3	045
14	B(a)	5.9	2	1.32, 2.21	017	N/A	1.4	3.9	064
15	B(a)	12.6	7	1.10, 1.53, 1.11, 1.26, 1.31, 1.46	065	589.6	15.2	1.8	082
16	B	8.3	6	1.19, 2.22, 1.19, 1.16, 1.58, 1.11	005	217.6	8.3	1.2	063

Table 2. Morphometric parameters of each alignment, B=Basaltic, B(a)=Hypothesized Basalt, calculations done while ignoring cones cut off by data edge.

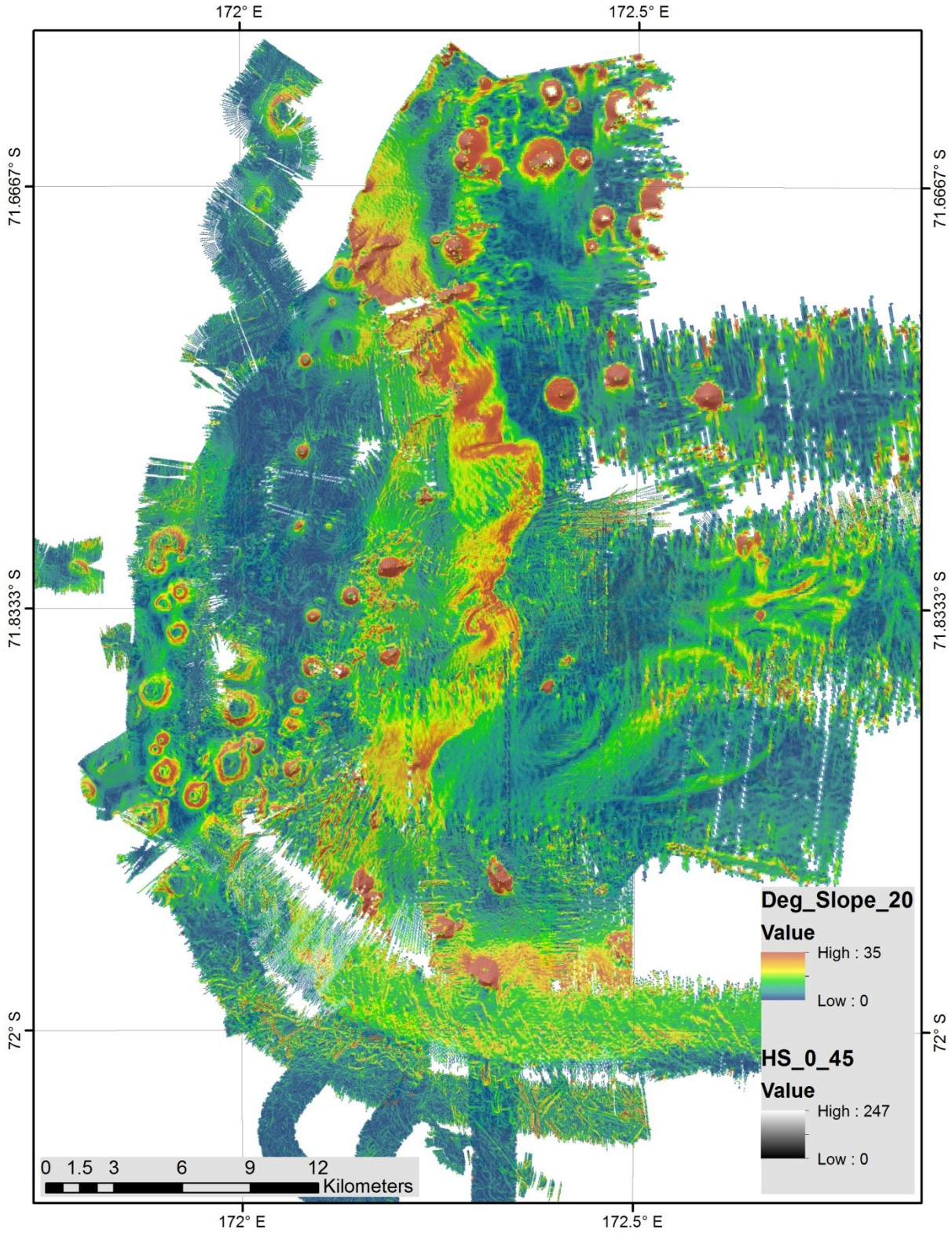

Figure 27. Slope map with hillshade underlay.

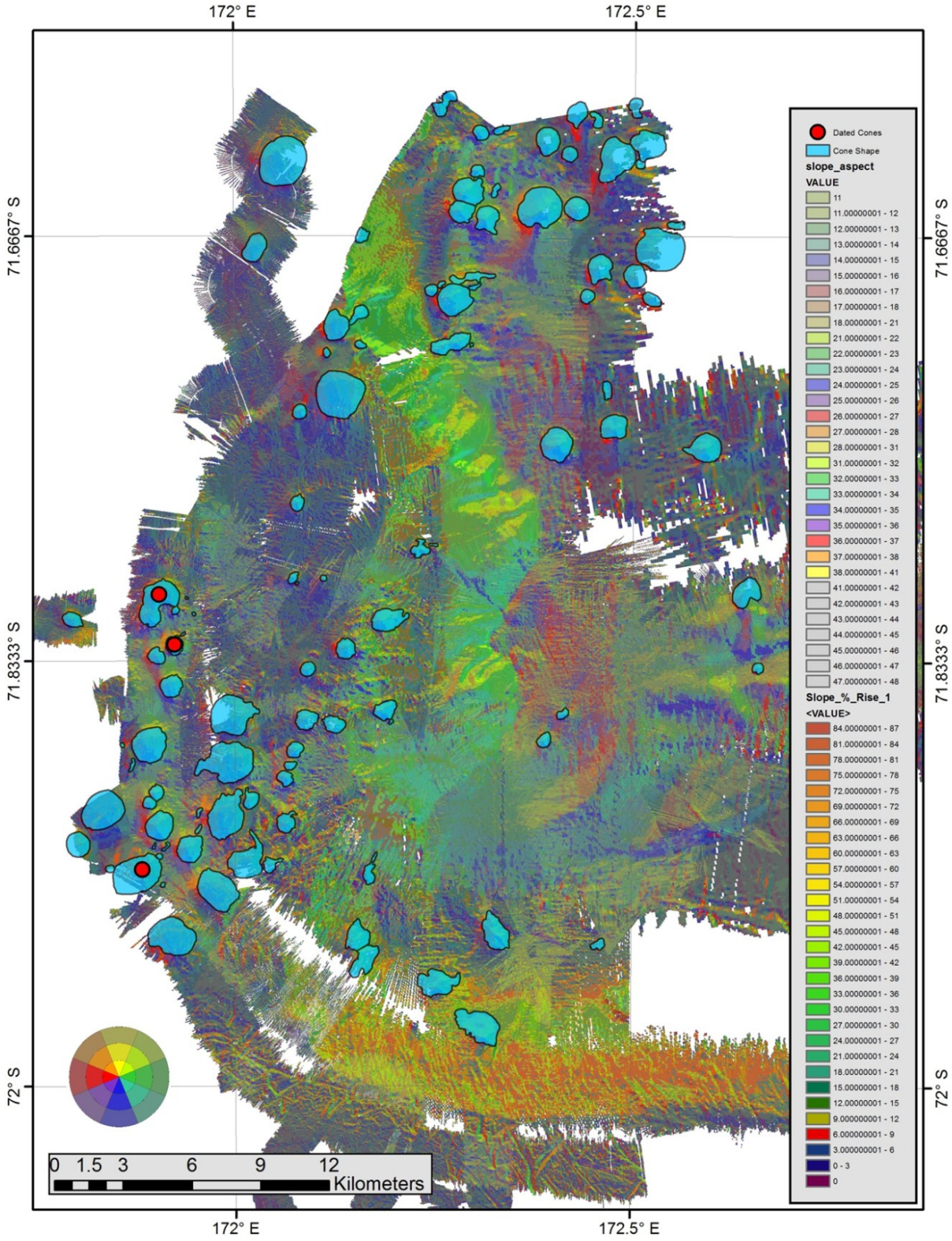

Figure 28. Slope aspect map with a custom color stretch, mapped cone bases and dredged cones.

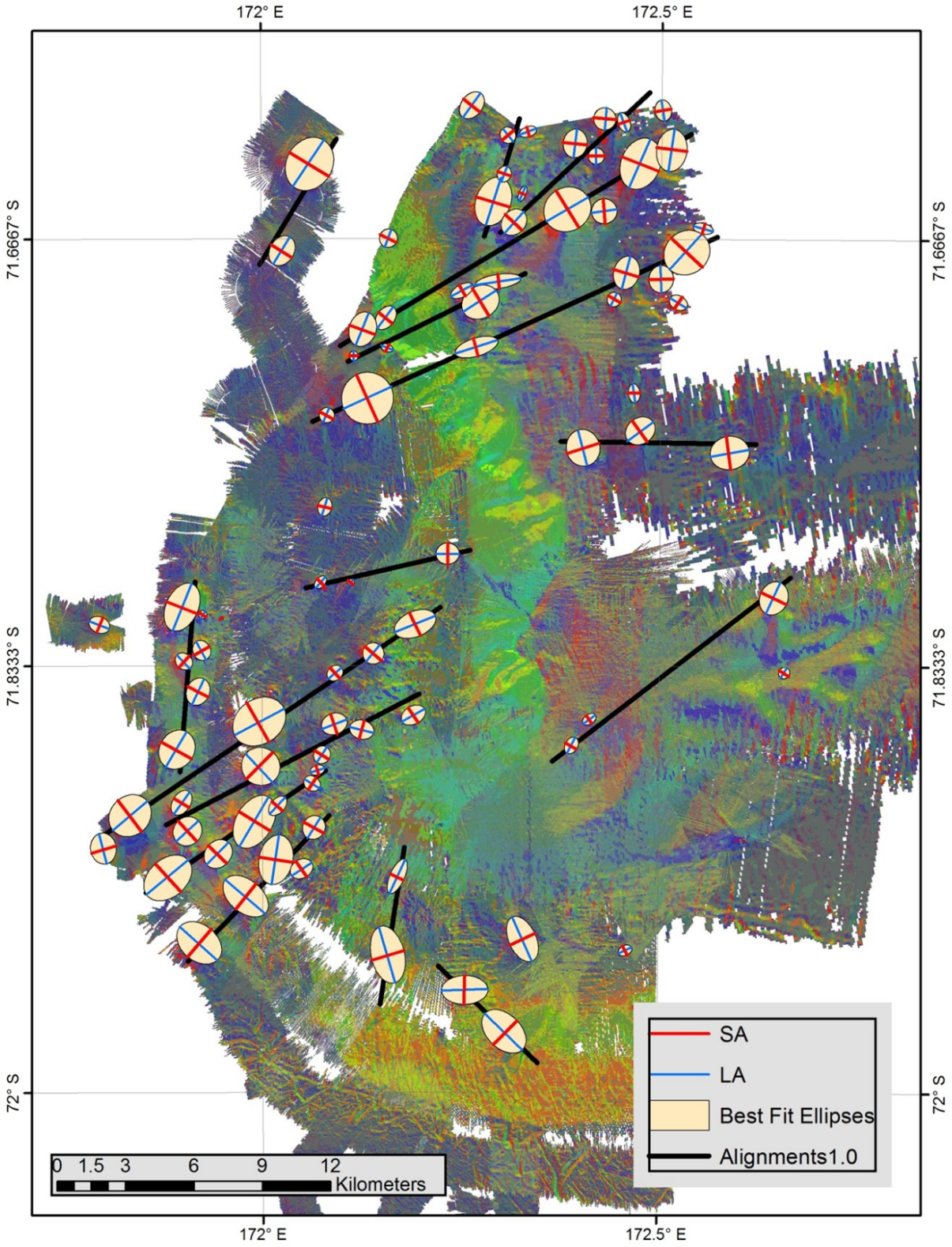

Figure 29. Slope aspect map revealing alignment trends, best fit ellipses and ellipse axes.

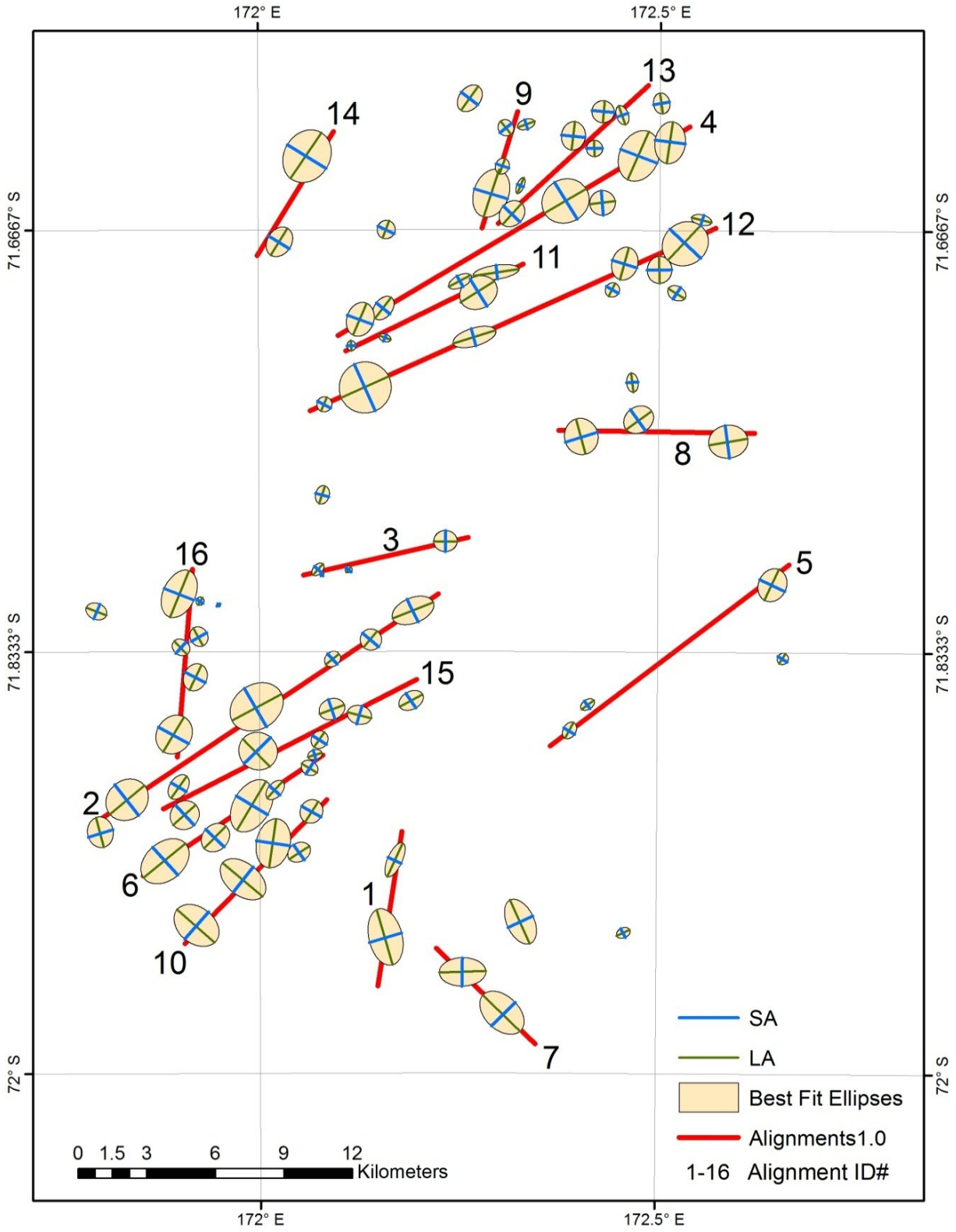

Figure 30. Best fit alignment map with assigned alignment ID #'s corresponding with table 2.

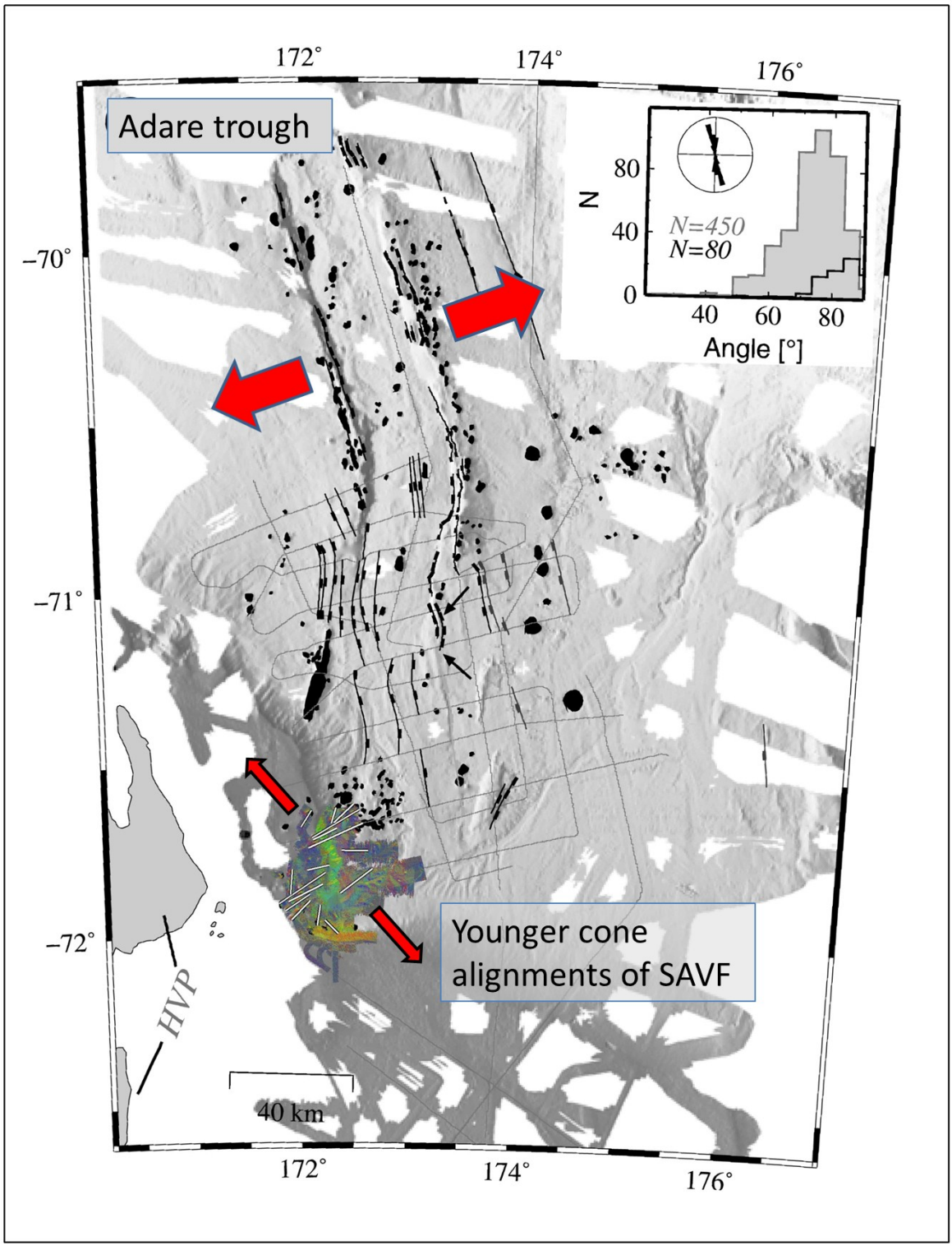

Figure 31. Adare trough documenting a NE-SW trend of minimum crustal stresses, and SAVF documenting a NW-SE trend of minimum crustal stresses [Modified from Granot et al., 2010].

Conclusions

For the Southern Adare Volcanic Field, I found a dominant NE-SW trend of aligned volcanic seamounts, documenting a NW-SE trend of minimum horizontal stress and a NE-SW trend of maximum horizontal stress in the crust. The average length of the 16 alignments proposed as fissures in this study is 9.98Km, the average azimuth of these alignments is 054º and the average vent long axis is 073º. The crustal stress direction determined in this study is at a high angle to previously documented volcanic trends around the Adare Trough [Granot, 2010] (Figure 31). The volcanic seamounts in the SAVF have a much younger age than the rift trends mapped by Granot et al. (2010). Therefore I can conclude that there has been a change to a new stress regime on the Ross Sea floor, Antarctica.

The methods used here were originally established by Paulsen and Wilson (2010). In this study the method was applied to seamounts. An improved method for mapping was developed, by mapping each cone base on a slope/aspect map with a custom color stretch, which more accurately shows the base of the cones. The cones mapped for this study are larger than the ones mapped by Paulson and Wilson (2010), so the morphometric parameters used to establish reliability grades are not accurate for this region. The parameters of the assessment system including the orthogonal distance from the best-fit line, the average vent spacing distance and, possibly, the number of vents need to be reconsidered for seamounts of the size that are typical in the SAVF and other similar regions.

Acknowledgements

This material is based on data provided by the Antarctic and Southern Ocean Data Portal (http://www.marine-geo.org/portals/antarctic/). The Marine Geoscience Data System provided the necessary GeoMapApp 3.3.0 tool which allowed me to view and download the bathymetric data. I would like to acknowledge NSF for supporting the Antarctic and Southern Ocean Data Portal and the Marine Geoscience Data System. I would also like to acknowledge MB-System for making the data processing possible and also the data acquisition on the *Nathanial B. Palmer.* I would also like to thank my research group for all their help and teachings; in particular Dr. Terry Wilson, Dr. Stephanie Konfal and Jie Chen, without them this research would not have been possible.

References

Adiyaman, Ö. et al. (1998). Relationships between volcanic patterns and neotectonics in Eastern Anatola from analysis of satellite images and DEM. *Journal of Volcanology and Geothermal Research, 85*, 17-32.

Anderson, E. M. (1951). The Dynamics of Faulting and Dyke Formation with Applications to Britain, 2nd edition. Oliver and Boyd, Edinburgh. 206 p.

Behrendt, J. C., & A. Cooper (1991), Evidence of rapid Cenozoic uplift of the shoulder escarpment of the Cenozoic West Antarctic rift system and a speculation on possible climate forcing, *Geology, 19*(4), 315–319.

Cande, S. C., and J. M. Stock (2005). Constraints on the timing of extension in the Northern Basin, Ross Sea, in Antarctica: Contributions to Global Earth Sciences, edited by D. K. Futterer et al., chapter 6.5, 319–326, Springer, New York.

Cande, S. C., J. M. Stock, D. Müller, and T. Ishihara (2000). Cenozoic motion between East and West Antarctica. *Nature, 404*, 145– 150.

Carbotte, S.M., W.B.F. Ryan, S. O'Hara, R. Arko, A. Goodwillie, A. Melkonian, R.A. Weissel, V.L. Ferrini, Antarctic Multibeam Bathymetry and Geophysical Data Synthesis: An On-Line Digital Data Resource for Marine Geoscience Research in the Southern Ocean, U.S. Geological Survey Open-File Report 2007-1047, doi:10.3133/of2007-1047.srp002, 2007.

Davey, F. J., and G. Brancolini (1995), The late Mesozoic and Cenozoic structural setting of the Ross Sea region, in Geology and Seismic Stratigraphy of the Antarctic Margin*, Antarctic Research Series, volume 68*, edited by A. K. Cooper, P. F. Barker, and G. Brancolini, pp. 167–182, AGU, Washinghton, D. C.

Delaney, P.T., Pollard, D.D., Ziony, J.I., McKee, E.H., (1986). Field relations between dikes and joints: emplacement processes and paleostress analysis. *Journal of Geophysical Research 91*, 4920–4938.

Deming (Model II) linear regression performed using GraphPad Prism version 6.00 for Windows, GraphPad Software, La Jolla California USA, www.graphpad.com.

Divenere, V. J., D. V. Kent, and I. W. D. Dalziel (1994), Mid-Cretaceous paleomagnetic results from Marie Byrd Land, West Antarctica: A test of post 100 Ma relative motion between East and West Antarctica, *Journal of Geophysical Research, 99* (B8), 15,115–15,139.

Fitzgerald,P.G.,M.Sandiford,P.J.Barrett,andA.J.W. Gleadow (1986), Asymmetric extension associated with uplift and subsidence in the Transantarctic Mountains and Ross Embayment, *Earth and Planetary Science Lett*ers, 81,67–78.

Granot, R., et al. (2010). Postspreading rifting in the Adare Basin, Antarctica: Regional tectonic consequences. *Geochemistry Geophysics Geosystems, 11*(8), 1-29.

Heidbach, O., & Höhne, J. (2008). CASMI-A visualization tool for the World Stress Map database. *Computers & Geosciences, 34*(7), 783-791.

LeMasurier, W. E. (1990), Late Cenozoic volcanism on the Antarctic Plate: An overview, in Volcanoes of the Antarctic Plate and Southern Oceans, *Antarctic Research Series, volume 48*, edited by W. E. LeMasurier and J. W. Thomson, pp. 1–17, AGU, Washinghton, D. C.

MacDonald, G.A., (1972). Volcanoes. Prentice Hall, Inc., Englewood Cliffs, New Jersey. 510 p.

Nakamura, K., (1977). Volcanoes as possible indicators of tectonic stress orientation principal and proposal. *Journal of Volcanology and Geothermal Research 2*, 1–16.

Paulson, T. S., & Wilson, T. J. (2010). New criteria for systematic mapping and reliability assessment of monogenetic volcanic vent alignments and elongate volcanic vents for crustal stress analyses. *Tectonophysics, 482,* 16-28.

Settle, M., (1979). The structure and emplacement of cinder cone fields. *American Journal of Science* 279, 1089–1107.

Van Der Pluijm, B. A. (2004) *Earth Structure.* New York, NY: W.W. Norton & Company Limited.